Archaeological and Anthropological Sciences (2022) 14:222
https://doi.org/10.1007/s12520-022-01686-0

ORIGINAL PAPER

# A micro-geoarchaeological view on stratigraphy and site formation processes in the Middle, Upper and Epi-Paleolithic layers of Sefunim Cave, Mt. Carmel, Israel

David E. Friesem[1,2] · Ron Shimelmitz[3] · Mara L. Schumacher[4,5] · Christopher E. Miller[4,6,7] · Andrew W. Kandel[8]

Received: 18 May 2022 / Accepted: 14 October 2022 / Published online: 11 November 2022


## Abstract

This paper presents a micro-geoarchaeological study carried out on the sedimentary sequence exposed at the entrance of Sefunim Cave, Israel, a sequence that spans from the Middle Paleolithic to the early Epipaleolithic periods. Using FTIR and micromorphological techniques, we investigated the stratigraphic sequence to reconstruct patterns of site use and archaeological formation processes. We identified formation processes that are common among Paleolithic caves sites in the Southern Levant, mainly the deposition of local *terra rossa* through colluvial sedimentation. Taphonomic disturbances of the deposits range from minimal to moderate, exhibited mainly by root and burrowing activity, but with no evidence for significant transport of archaeological materials. While the upper layers (II–III) are decalcified, the precipitation of secondary calcite results in increasing cementation of the sediments with depth in the lower layers (V–VII). We observed variation at the microscopic scale and identified an inverse correlation between human and carnivore activity throughout the layers. We observed human activity by the presence of micro-archaeological materials such as chert, bone, charcoal, rubified clay, burnt bone and shell, and wood ash. We observed carnivore activity by the presence of phosphatic grains and coprolite fragments as well as chewed and digested bones. We conclude that human activity at the site was characterized by episodes of varying intensity, based on the frequency of archaeological finds within the different layers. The alternating episodes of human and carnivore activity at Sefunim Cave may demonstrate the close-knit interactions and reciprocal relations that humans and carnivore shared at Paleolithic caves.

**Keywords** Paleolithic Caves · Southern Levant · Fire · Hyenas · Micromorphology · FTIR

✉ David E. Friesem
dfriesem@univ.haifa.ac.il

Ron Shimelmitz
rshimelmi@staff.haifa.ac.il

Mara L. Schumacher
m.l.schumacher2@newcastle.ac.uk

Christopher E. Miller
christopher.miller@uni-tuebingen.de

Andrew W. Kandel
a.kandel@uni-tuebingen.de

1 Department of Maritime Civilizations, Recanati Institute of Maritime Studies, School of Archaeology and Maritime Cultures, University of Haifa, 3498838 Haifa, Israel

2 Haifa Center for Mediterranean History, University of Haifa, Mount Carmel, 31905 Haifa, Israel

3 Zinman Institute of Archaeology, School of Archaeology and Maritime Cultures, University of Haifa, Mount Carmel, 31905 Haifa, Israel

4 Institut Für Naturwissenschaftliche Archäologie, Eberhard-Karls-Universität Tübingen, Hölderlinstr. 12, 72074 Tübingen, Germany

5 School of History, Classics and Archaeology, Newcastle University, Newcastle upon Tyne NE1 7RU, UK

6 Senckenberg Centre for Human Evolution and Paleoenvironment, University of Tübingen, Hölderlinstr. 12, 72074 Tübingen, Germany

7 SFF Centre for Early Sapiens Behaviour (SapienCE), University of Bergen, Postboks 7805, NO-5020 Bergen, Norway

8 The Role of Culture in Early Expansions of Humans (ROCEEH), Heidelberg Academy of Sciences & Humanities, University of Tübingen, Hölderlinstr. 12, 72074 Tübingen, Germany

## Introduction

Sefunim Cave, Mount Carmel, Israel, provides a window into behavioral changes during the Late Pleistocene (Ronen 1984; Shimelmitz et al. 2018). The cave's cultural sequence includes layers from the late Middle Paleolithic (MP) to the Epipaleolithic (EP) and enables us to examine changes in the relationship between humans and their environment. Additionally, the sequence provides an important window into questions of population dispersal and expansion of human groups and their resulting interactions, as existing models postulate for the Initial Upper Paleolithic (IUP), the early Upper Paleolithic (UP), and the Levantine Aurignacian (LA) (Goring-Morris and Belfer-Cohen 2006; Belfer-Cohen and Goring-Morris 2012; e.g., Alex et al. 2017).

The objective of this study is to investigate the archaeological formation processes of the different stratigraphic units of the cave with an aim to define the changing depositional and post-depositional processes as well as the nature of human occupation in the cave. To achieve this, we applied a micro-geoarchaeological approach, analyzing the deposits uncovered within the newly excavated sedimentary sequence (Shimelmitz et al. 2018). We examined different sedimentary units in order to better characterize and refine the site's stratigraphy. The results provide a detailed framework for the site's formation processes and show how each stratigraphic unit reflects shifting intensities of human activity as well as changing taphonomic processes.

### Background

Sefunim Cave is situated in Mount Carmel, a region rich in carbonate rocks, which reaches an elevation of 524 m above current sea level and is cut by a series of channels, primarily running from east to west. The cave formed in Cretaceous age rocks (Ronen 1984: 21, Fig. 2.2). Clay-rich *terra rossa* soils are common throughout this landscape (Singer 2007). Sefunim Cave is located along the southern bank of Nahal (wadi) Sefunim at an elevation of 125 m above sea level about 800 m east of the 2-km-wide coastal plain, but its distance to the Mediterranean would have varied as past sea levels changed (Fig. 1a). This karstic cave complex consists of a massive front chamber with an overall length of about 50 m, a smaller inner chamber, and a narrow terrace located near the northeastern entrance of the cave (Figs. 1b, 2). Outside the main entrance of the cave lie massive limestone boulders resulting from the partial collapse of the cave's front during the Holocene. More limestone boulders are strewn inside the cave, some of which are completely or partly buried within the Late Pleistocene sediments, indicating earlier episodes of collapse of the cave roof and walls.

M. Stekelis (1961) first investigated the site in 1941. He dug a small trench of 3 $m^2$ located near the northeastern entrance and reported the presence of UP, EP, and Neolithic (NEO) finds in four horizons (A–D). Between 1965 and 1970, A. Ronen performed extensive excavations across most of the cave complex. His excavations covered about 90 $m^2$ within the front chamber and 15 $m^2$ on the terrace. He documented 13 layers (1–13) within the front chamber, but identified a different stratigraphic sequence on the terrace (I–VII). Ronen (1984) described occupation horizons from the MP, UP, EP, NEO, and even historical periods. He recognized that MP and UP sediments were preserved mainly near the cave's entrance around large collapsed boulders. While Ronen's team removed some of the rocks to access the underlying deposits, they left most of them in place, preserving a considerable volume of sediment underneath.

Farrand (1984) analyzed the sediments exposed during the excavations of Ronen and concluded that the main source of sediments in the cave is aeolian silt from the nearby coastal plain mixed with local *terra rossa*. He argued that the weathering of stones was related to chemical dissolution and identified decalcification of the upper sediments and cementation, due to the reprecipitation of calcite, in the lower layers. Last, Farrand (1984) identified different rates of deposition and intensity of post-depositional diagenesis in the rear of the cave, as opposed to the entrance.

### The renewed excavation

A team from the Universities of Haifa and Tübingen conducted excavations in 2013, 2014, 2015, and 2017, while analysis of the finds and sediment has continued since then. The excavations focus on an area of about 12 $m^2$ just inside the cave's entrance and represent the focus of this geoarchaeological investigation (Figs. 1b and c, 2). Since Shimelmitz et al. (2018) present details about excavation methods and stratigraphy, we provide a summary of the seven archeological horizons (AH) found at this part of the cave, from AH I to VII. (Note that these layers are not related to Ronen's sequence on the terrace.) AHs were defined in the field based on sedimentological differences observed through changes in color and texture. Though some variations were detected in each AH, these were challenging to observe with the naked eye alone, and we therefore initiated the micro-geoarchaeological study to better define each AH.

The surface layer is known as AH I and ranges from 5 to 15 cm thick. Since AH I represents disturbed sediments on the cave floor, we do not address this layer any further. Two separate pits are assigned to AH II and represent localized intrusions into deeper layers. The first pit, AH IIa, is filled with decalcified, dark brown silty clay and contains finds

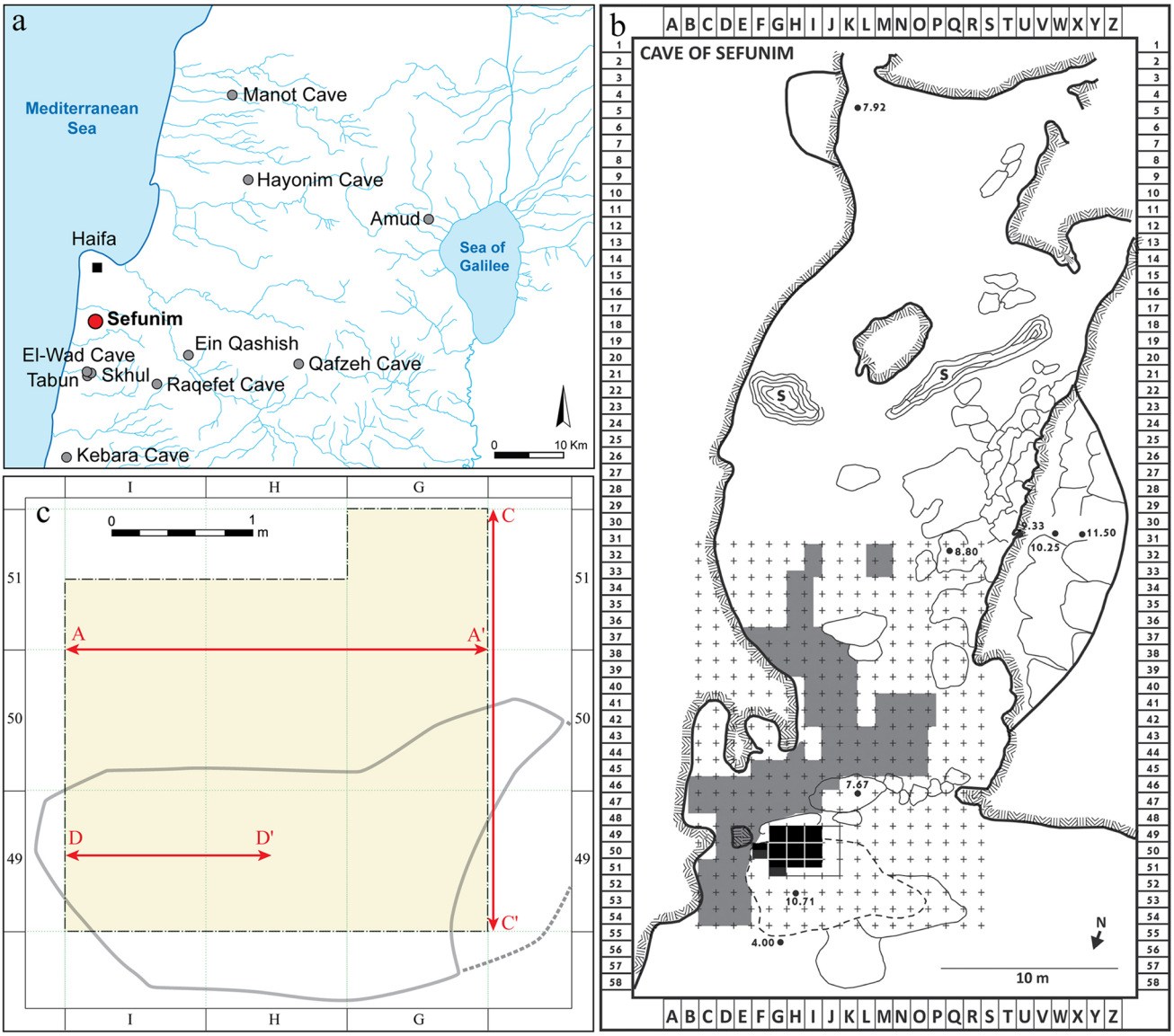


**Fig. 1** Site location and plan. **a** A map of modern-day Northern Israel showing the location of key Paleolithic cave sites (modified after Yeshurun et al. 2021: Fig. 1). **b** A plan of the cave showing in gray the area excavated by Ronen (1965–1970) and in black the area of the renewed excavations (2013–2017) (modified after Ronen 1984:112). **c** A view of the grid map of the renewed excavation area. Red lines mark the locations of the profiles shown in Fig. 2, and gray line depicts original position of "Three-Drill Rock" (graphic made using ESRI ArcMap 10.6.1)

associated mainly with the EP (Shimelmitz et al. 2018). It consists of a shallow, saucer-shaped lens with a maximum thickness of 20–25 cm in units G50–G51, thinning to the west. The second pit, AH IIb is a pot-shaped pit about 50 cm deep with straight walls that extend down to AH V. The pit contains many large stones infilled with dark clayey sediment, which hindered the collection of block samples and precluded micromorphological examination.

AH III is the first laterally extensive stratigraphic unit identified during the excavation. This layer yielded a high amount of fauna and lithics. The lithic industry of AH III was attributed to the Kebaran of the early EP period, dated by OSL to 24–21 ka (Shimelmitz et al. 2018). AH III is composed of decalcified, very compact, dark brown silty clay.

AH IV is noticeably lighter in color than AH III, with a gradual transition. Similar to AH III, AH IV is present across the entire excavation, but contains fewer lithics and bones. The lithic industry was attributed to the Late UP (Shimelmitz et al. 2018), dated by OSL to $27 \pm 1$ ka (Slon et al. 2022). AH IV consists of firm brown to yellowish-brown silty clay with some UP artifacts, becoming more calcified with depth.

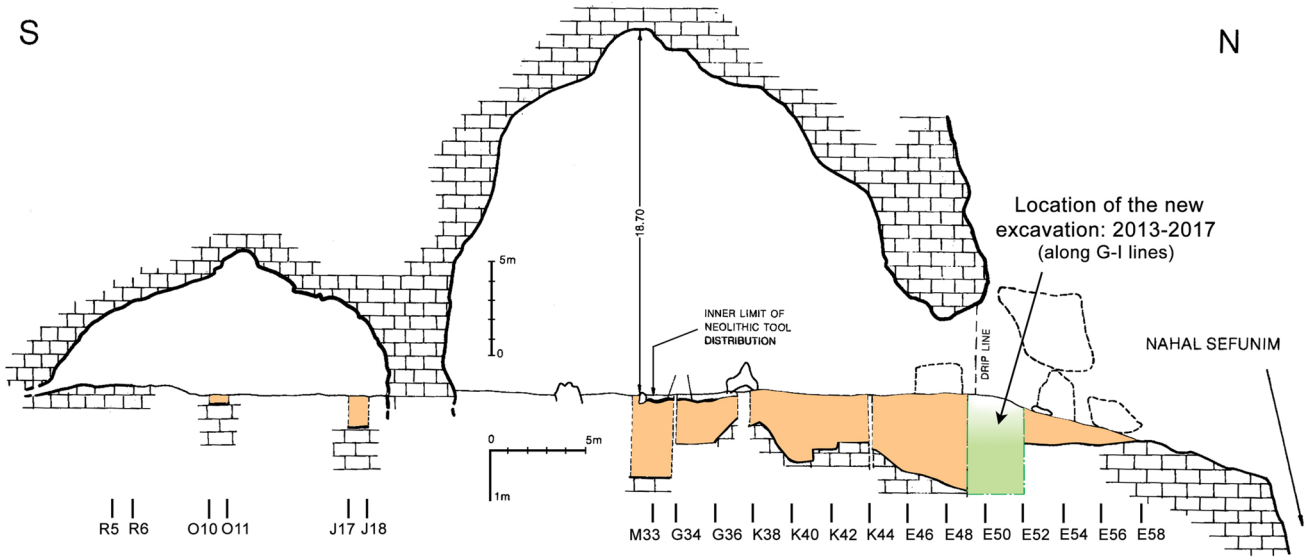


**Fig. 2** Illustrations showing the south-north section of the cave, the location of Ronen's excavation (1965–1970, orange shading), and the new excavation (2013–2017, green shading) (graphic is after Ronen 1984: 83, Fig. 6.2)

AH V is light yellowish-brown and can be traced across the excavation. It includes bones, lithics, and marine shells which were attributed to the LA industry of the early UP (Shimelmitz et al. 2018), dated by radiocarbon to 30–40 ka (Slon et al. 2022). The sediment in AH V is a carbonate-rich, very compact, clayey silt, which becomes more calcified with depth. AH V contains variable amounts of limestone and dripstone, evidence for a gradual collapse of the cave's roof (Fig. 2).

AH VI is a compact, reddish-yellow clayey silt. While the layer appears to extend across the excavation, only a part of it is currently exposed. Compared to the other layers, AH VI exhibits a low concentration of bones and lithics. Although lithics are not common, they look different from those of the overlying layer and include rare Levallois and Levallois-like artifacts. In accordance to its stratigraphical position, the palimpsest of this layer represents a time frame that is assumed to range from the MP to the early UP. The possibility that this horizon includes the IUP was already noted by Ronen (1984). Emireh points, typical of the IUP, are known from Sefunim. In Ronen's excavation, these points were not found in context, with one each from the UP and NEO layers, while in Stekelis' excavation, one comes from Layer D underlying the Levantine Aurignacian level. This layer was dated by OSL to $51 \pm 3$ ka (Slon et al. 2022).

The lowest layer excavated so far is AH VII, exposed in just a limited part of units G48–G50. The sediment is light brown and partly cemented. Preliminary analysis of the lithic industry from this layer indicates it is associated with the MP, as evidenced by the prevalence of Levallois technology, dated by OSL to $71 \pm 4$ ka (Slon et al. 2022). Many bones are present in this layer as well.

A very large boulder (ca. $3 \times 2 \times 1.5$ m) divided the excavation into two parts, with the largest area on its north side. Ronen named the boulder "Three-Drill Rock," following his failed attempts to remove it (Fig. 1c). On its south side, we initially added the letter "A" to the layer names because we could not confirm that the layers continued. Finally, in 2017, we succeeded in removing the boulder, which allowed us to link the stratigraphy. Therefore, we report the north and south parts of each layer as a single entity. Since Three-Drill Rock rested on the upper part of AH III, we place its fall at the end of the Late Pleistocene.

## Materials and methods

### Sampling strategy

At the end of each season, the team collected undisturbed monolithic sediment blocks from AH II–VII for micromorphological analysis ($n = 20$; Table 1 and Fig. 3). Two further blocks were collected outside the cave as control samples for reference to natural sediments and soils without anthropogenic influence. The first sample was collected on the hillslope 40 m above the cave from brownish-red *terra rossa* found between crevasses in the limestone bedrock that forms the Mount Carmel landscape. The second was collected 20 m below and east of the cave along the banks of Nahal Sefunim.

As part of the systematic sampling strategy, the team also collected 250 bulk sediment samples during the excavation. A typical bulk sample consisted of an $8 \times 12$ cm zip-lock bag, half-filled with loose sediment taken from every 2–3 cm

**Table 1** List of undisturbed sediment block samples and their location. Sample denotes year and number

| Sample | Square | Profile | Elevation (masl) | Layer |
|---|---|---|---|---|
| 13–1 | G50 | North | 601–611 | IV–V |
| 13–2 | G50 | North | 609–622 | III–IV |
| 13–3 | G50 | North | 625–635 | III |
| 13–4 | G50 | North | 618–629 | II–IV |
| 13–5 | G50 | North | 601–617 | IV–V |
| 14–1 | Control sediment sample above the cave | | | |
| 14–2 | Control sediment sample below the cave | | | |
| 14–3 | H50 | North | 585–603 | IV–V |
| 14–4 | G51 | East | 598–621 | IV–V |
| 15–1 | G51 | West | 590–611 | IV–V |
| 15–2 | G51 | West | 571–585 | V |
| 15–3 | G51 | West | 564–574 | V |
| 15–4 | G50 | North | 539–562 | V–VI |
| 15–5 | H51 | North | 597–616 | III–IV |
| 15–6 | H51 | North | 574–591 | V |
| 15–7 | H50 | North | 545–560 | V |
| 15–8 | G49 | East | 521–546 | VI |
| 15–9 | H50 | South | 587–610 | III–IV |
| 15–10 | H50 | South | 574–586 | V |
| 17–1 | I49 | North | 557–573 | IV–V |
| 17–2 | G49 | South | 502–518 | VI |
| 17–3 | G49 | East | 497–515 | VII |

spit in each square. The bulk samples provided a record of the sediment encountered and served as a source for sedimentological analyses.

## Fourier-transform infrared (FTIR) spectroscopy

FTIR analysis was performed in the Microanalytics Laboratory at the Institute for Archaeological Sciences at Tübingen University. The study was carried out using an Agilent Technologies Cary 660 infrared spectrometer equipped with a diamond crystal attenuated total reflectance (GladiATR) accessory. Absorbance spectra were obtained from powdered samples at a resolution of 4 $cm^{-1}$ for 36 scans in the 4400–400 $cm^{-1}$ spectral range. All obtained spectra were analyzed and processed using the Agilent Resolution Pro and Essential FTIR software packages. The spectra were then compared to internal and RRUFF™ reference databases for identification.

The 250 bulk samples collected in the field were subsampled in the lab based on texture, color, and size, in order to detect heat-induced changes in the crystal structure of the bones, shells, and clays that were present in the bulk samples. The analysis of 1209 subsamples focused on the differentiation of calcined and uncalcined bones, aragonite and calcite shells, and altered and unaltered clays. We note that within this analysis, it was not possible to distinguish differences in marine, freshwater, or terrestrial shell fragments. Therefore, in this paper, we use "shell" as a general term.

Calcined bones were determined based on peaks at 1088 and 631 $cm^{-1}$, forming at 600 °C or more, as a result of the decomposition of carbonates (Surovell and Stiner 2001; Thompson et al. 2009, 2013). Shells that experienced full or partial heat-induced transformation of aragonite into calcite were identified by their characteristic peak positions at 1454 $cm^{-1}$ (*v3*), 1082 $cm^{-1}$ (*v1*), and 856 $cm^{-1}$ (*v2*) as well as the peak doublet at 712/700 $cm^{-1}$ (*v4*) (Toffolo and Boaretto 2014; Loftus et al. 2015). Identification of heat-altered clays was based on the absence of absorptions bands of O–H functional groups and structural water in the 3600 and 3400 $cm^{-1}$ regions, respectively, as well as the shift of the main peaks from ca. 1030 $cm^{-1}$ to higher wavenumbers (Madejová 2003; Berna et al. 2007; Forget et al. 2015). Results of the FTIR analysis of bulk sediment samples are summarized in Table 2 and Fig. 4.

## Micromorphology

During excavation, the undisturbed monolithic sediment blocks were carefully extracted and jacketed using plaster bandages. The blocks were transported to the Geoarchaeology Laboratory at the University of Tübingen where they were dried in an oven at 40 °C for 24 h and then impregnated under vacuum in a mixture of unpromoted polyester resin (Viscovoss), styrene, and a hardener of methyl ethyl ketone peroxide. Once the mixture had achieved a gel-like consistency, the samples were heated again at 40 °C overnight. The hardened blocks were then sliced and subsampled for thin sectioning. The 30-µm-thick sections ($n = 43$) measuring 60 × 90 mm were prepared by P. Kritikakis of the Micromorphology Laboratory at the University of Tübingen. The thin sections were studied under the naked eye and under magnification (25–200X) using a Zeiss Axio Imager petrographic microscope with plane-polarized light (PPL), cross-polarized light (XPL), and blue-light fluorescence. Micromorphological description follows the terminology of Stoops (2003) and is presented in Table 3. We made a qualitative assessment of each thin section in order to evaluate the relative abundance of: (1) fire residues, including rubified clay aggregates, microcharcoal, wood ash pseudomorphs and burnt bones; (2) microchert (< 2 mm); (3) shell fragments; (4) phosphatic grains; (5) micro-bones (< 2 mm); and (6) the extent of calcitic cementation of the matrix (Table 4 and Fig. 5).

## Fourier-transform infrared microspectrometry (micro-FTIR)

Representative thin sections ($n = 9$) from each layer were analyzed using an Agilent Cary 610 FTIR microscope in

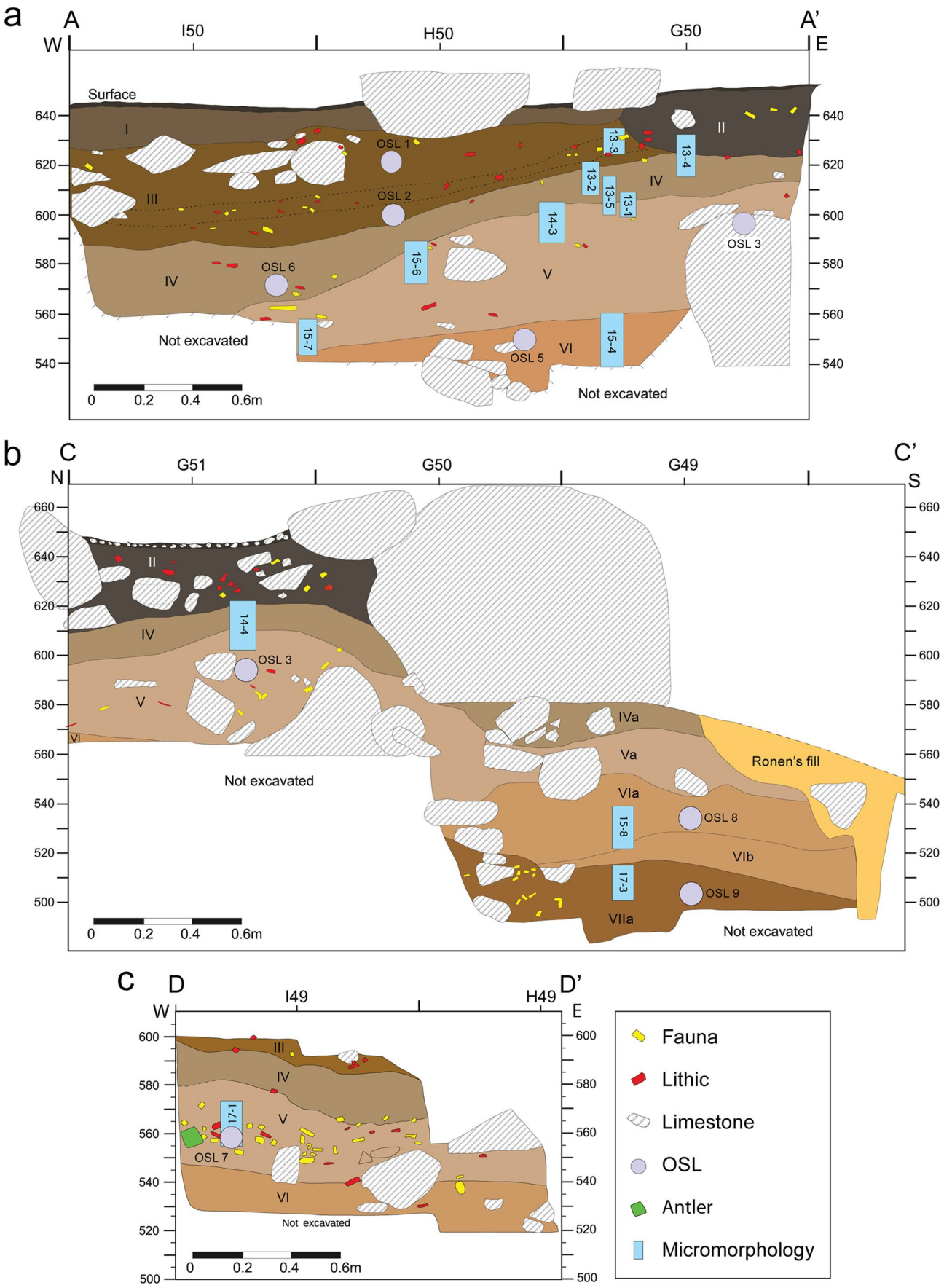
a
A
I50
H50
G50
A'
W
E
Surface
I
II
III
IV
V
VI
OSL 1
OSL 2
OSL 3
OSL 5
OSL 6
13-1
13-2
13-3
13-4
13-5
14-3
15-4
15-6
15-7
Not excavated
Not excavated
0 0.2 0.4 0.6m
b
C
G51
G50
G49
C'
N
S
II
IV
V
VI
14-4
OSL 3
IVa
Va
VIa
VIb
VIIa
Ronen's fill
15-8
17-3
OSL 8
OSL 9
Not excavated
Not excavated
0 0.2 0.4 0.6m
c
D
I49
H49
D'
W
E
III
IV
V
VI
17-1
OSL 7
Not excavated
0 0.2 0.4 0.6m
Fauna
Lithic
Limestone
OSL
Antler
Micromorphology

◂**Fig. 3** Illustrations showing the location of major stratigraphic units and block sediment samples. **a** Profile A-A'. **b** Profile C–C'. **c** Profile D-D'. See Fig. 1c for profile locations on the site grid plan (graphic made using CorelDRAW X7)

order to identify mineral components and the extent of their alteration. Measurements were conducted using the transmission method with 64 scans. All spectra were obtained at 4 $cm^{-1}$ resolution using Agilent Resolution Pro software and interpreted using an internal library of infrared spectra for archaeological materials. In order to examine the exposure of the sediments to high temperature, the extent of clay alteration was estimated following Berna et al. (2007) modified to use via micro-FTIR (Villagran et al. 2017; e.g., Friesem et al. 2020). In total, 17 infrared spectra were collected (Table 5 and Fig. 6).

## Results

### Control sediments

The sediment samples collected from above and below the cave served as a control for the natural environment. These display a granular structure due to the activity of roots and microfauna. A difference in color can be seen, with the sediment below the cave being darker brown, while the sediment above the cave exhibits a stronger brownish-red color. Micromorphological observations indicate that the natural sediments are characterized by rounded peds, open microstructure, organic black residues, and iron staining in the clay-rich groundmass (Fig. 7a). Silt to fine-sand sized, subangular quartz grains comprise 5–10%, likely originating as aeolian deposition from the nearby coastal plain. The sediments also contain shell fragments, likely as a result of land snails, some calcite in the groundmass, and limestone fragments in initial dissolution. The rounded peds structure indicates soil formation following colluvial deposition. FTIR analysis of the sediment showed clay minerals, calcite, and quartz to be the major components (Fig. 4a). Analysis of the clay-rich groundmass under the micro-FTIR displayed prominent absorption bands at 3620 and 3695 $cm^{-1}$. These bands are attributed to the clay's structural water (O–H bands) and show no alteration of the clay. Therefore, we interpret this clay as unburnt (Table 5 and Fig. 6a).

### AH II

This layer consists of two pits and thus displays localized intrusions of younger materials into older layers. Under the microscope, the sediment from AH IIa showed a complex microstructure with large channels (Fig. 7b). The groundmass is rich in clay with silt to medium-sand sized angular quartz at 10% abundance. Bone fragments vary in color, ranging from yellow to white. Overall, the sediments seem decalcified, despite the presence of a few limestone fragments (Table 4 and Fig. 5).

### AH III

Micromorphologically, the sediments associated with AH III are composed of a decalcified, clay-rich groundmass. However, some calcite was identified in the groundmass near limestone fragments. Channels seem to be the most dominant void type within the overall dense and massive microstructure of the sediments (Fig. 7c). Silt to medium-sand sized sub-angular quartz is found at 5–10% abundance (Fig. 8a–b). The sediments of AH III present a very high abundance of bone and chert fragments, some with signs of burning, as further supported by FTIR analysis. For instance, white colored bones display masked birefringence, which hints at these being calcined as a result of burning. Dark

**Table 2** FTIR results: absolute and relative abundance of bone, shell and clay in respective level. Heat-altered shells include aragonite-calcite shells and pure calcite shells

| Layer | Uncalcined bone | | Calcined bone | | Aragonite shell | | Heat-altered shell | | Unaltered clay | | Altered clay | | Number of analyzed bones, shell and clay in subsamples (*n*) |
|---|---|---|---|---|---|---|---|---|---|---|---|---|---|
| | *n* | % | *n* | % | *n* | % | *n* | % | *n* | % | *n* | % | |
| II | 4 | 100.0 | - | - | - | - | - | - | - | - | - | - | 4 |
| III | 21 | 70.0 | 2 | 6.7 | 5 | 16.7 | 1 | 3.3 | - | - | 1 | 3.3 | 30 |
| III–IV | 1 | 100.0 | - | - | - | - | - | - | - | - | - | - | 1 |
| IV | 48 | 69.6 | 5 | 7.2 | 7 | 10.1 | 4 | 5.8 | 4 | 5.8 | 1 | 1.4 | 69 |
| IV–V | 61 | 64.2 | 5 | 5.3 | 19 | 20.0 | 5 | 5.3 | 4 | 4.2 | 1 | 1.1 | 95 |
| V | 114 | 64.0 | 12 | 6.7 | 38 | 21.3 | 3 | 1.7 | 8 | 4.5 | 3 | 1.7 | 178 |
| VI | 79 | 85.9 | 3 | 3.3 | 6 | 6.5 | 1 | 1.1 | 2 | 2.2 | 1 | 1.1 | 92 |
| VII | 43 | 95.6 | 1 | 2.2 | - | - | - | - | 1 | 2.2 | - | - | 45 |
| Σ | 371 | 72.2 | 28 | 5.4 | 75 | 14.6 | 14 | 2.7 | 19 | 3.7 | 7 | 1.4 | 514 |

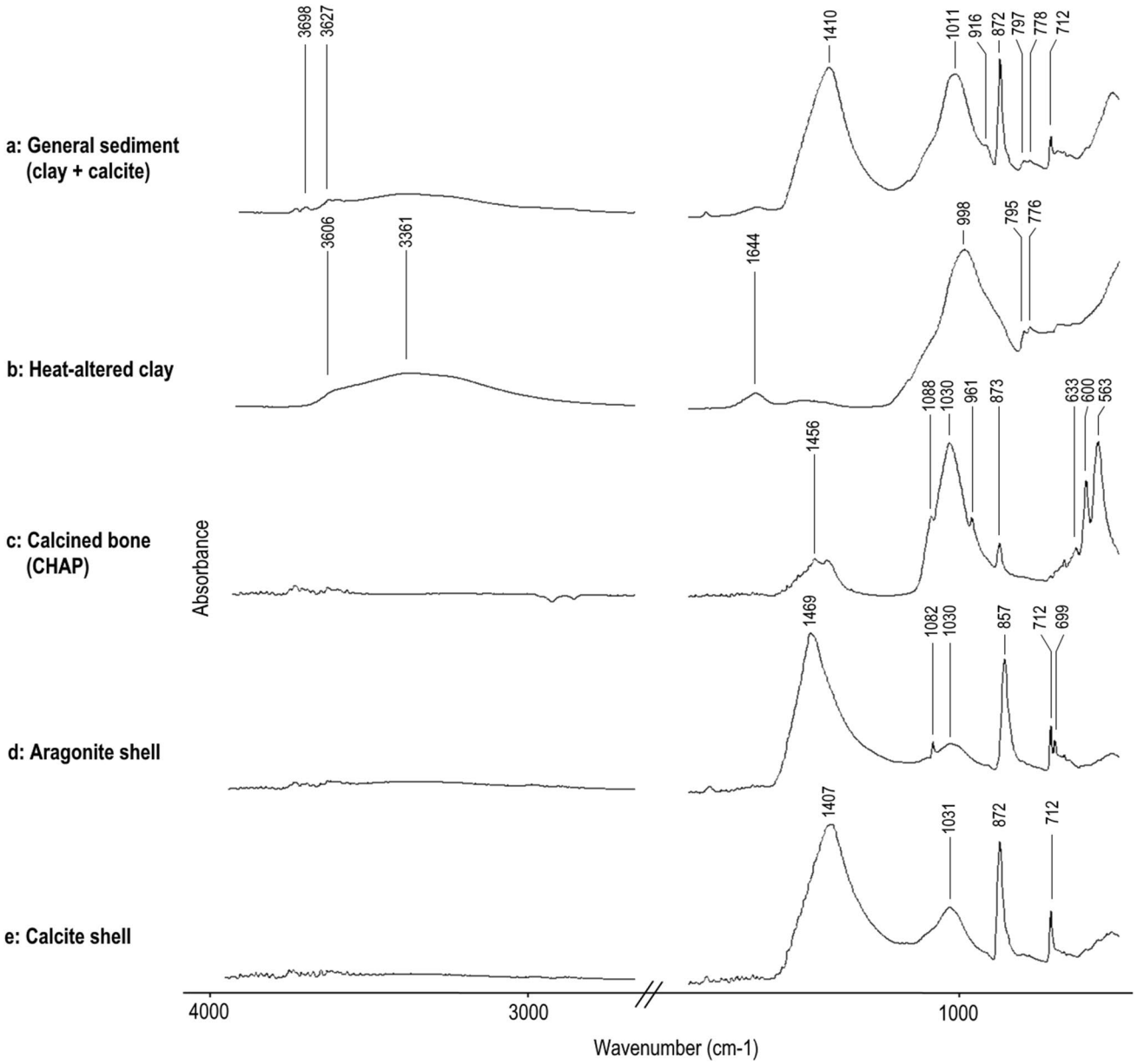


**Fig. 4** ATR spectra of selected archaeological materials from Sefunim Cave. **a** general sediment showing clay (3698, 3627, 1011, 916, 797, and 778 $cm^{-1}$) and calcite (1410, 872, and 712 $cm^{-1}$) as major mineral components. **b** Low-temperature heated clay, note the weak peak in the 3600 $cm^{-1}$ region indicative of a loss of structural water induced by heat alteration. **c** Calcined bone (CHAP) with characteristic peaks at 1456, 1088, 1030, 961, and 633 $cm^{-1}$ indicating heating to > 500 °C. **d** Aragonite shell (1469, 857, 712, 699 $cm^{-1}$) with some sediment (1082, 1030, 712 $cm^{-1}$) attached to the shell. **e** Calcite shell (1407, 872, 712 $cm^{-1}$) with some clay (1031 $cm^{-1}$) attached to the shell

reddish-brown clay aggregates suggest rubification following exposure to high temperatures. Fire residues observed under the microscope also include wood ash pseudomorphs and micro-charcoal (Table 4, Fig. 5). A few phosphatic grains were observed, but at a relatively low abundance (Fig. 8a–b). A granostriated b-fabric was found around grains, aggregates, chert, and bone fragments (Fig. 8a–d). FTIR analysis of sediments indicated that some clays were altered by exposure to elevated temperature (Table 2 and Fig. 4b). A few bones were identified as calcined (Table 2 and Fig. 4c). Aragonitic shells were also identified via FTIR (Table 2 and Fig. 4d) alongside heat-altered shells composed of calcite (Table 2 and Fig. 4e). Micro-FTIR analysis of the sediments' clay-rich groundmass exhibited prominent O–H absorption bands at 3620 and 3695 $cm^{-1}$, typical of unaltered clay. However, these absorption bands were absent in the analysis of a dark reddish-brown clay aggregate, indicating the alteration of clay due to exposure to elevated

**Table 3** Summary of micromorphology analysis

| Layer | Industry/period | Field description | Microscopic features | Interpretation |
|---|---|---|---|---|
| I | Modern | Thin surface of fine brown-gray silty clay | Not studied | Recent (modern) activities |
| II | EP | Thick lens of fine black-gray silty clay | • Clay-rich groundmass<br>• Silt to medium sand size angular quartz at 10% abundance<br>• Bone fragments in various colors ranging from yellow to white<br>• Moderate amounts of fire residues, shells, and lithics<br>• Moderate amounts of phosphatic grains<br>• Intensive bioturbation<br>• Decalcification | Heavily disturbed mixed layer |
| III | Kebaran/Early EP | Loamy dark brown | • Clay-rich groundmass<br>• Silt to medium sand size sub-angular quartz at 5–10% abundance<br>• Bone fragments in various colors ranging from yellow to white, some with masked birefringence, some calcined<br>• Dark brown-reddish clay-rich aggregates, altered due to exposure to temperatures > 500 °C<br>• Very high abundance of fire residues, lithics, and shells (some transformed from aragonite to calcite)<br>• Few phosphatic grains<br>• Granostriated b-fabric<br>• Decalcification<br>• Bioturbation | Human activity, associated with pyrogenic activity |
| IV | Late UP | Loamy light brown | • Clay-rich groundmass<br>• Silt to medium sand size sub-angular quartz at 10% abundance<br>• High abundance of phosphatic grains and bone fragments in various colors ranging from yellow to white, some with masked birefringence<br>• Carnivore coprolites fragments<br>• Granostriated b-fabric<br>• Moderate to low amounts of fire residues, lithics, and shells<br>• Bioturbation<br>• Dissolution of limestone | Carnivore activity and reduced and/or more ephemeral human activity in the cave based on few localized fine layers showing moderate concentrations of materials associated with human activity |
| V | Levantine Aurignacian/Early UP | Loamy brown-yellow | • Clayish groundmass cemented with secondary calcite<br>• Limestone dissolution and precipitation of calcite cementing the matrix, in some few cases dissolution occur with phosphatization<br>• Silt to medium sand size sub-angular quartz at 10% abundance<br>• Bone fragments in various colors ranging from yellow to white, some with masked birefringence and in association with wood ash pseudomorphs, some calcined<br>• Moderate to low abundance of phosphatic grains<br>• Very high abundance of fire residues, lithics and shells (some transformed from aragonite to calcite)<br>• Granostriated b-fabric<br>• Bioturbation | Intensive human activity, associated with pyrogenic activity |

**Table 3** (continued)

| Layer | Industry/period | Field description | Microscopic features | Interpretation |
|---|---|---|---|---|
| VI | UP—MP | Loamy light brown | • Calcitic-clay groundmass<br>• Silt to medium sand size sub-angular quartz at 10% abundance<br>• High abundance of phosphatic grains<br>• Carnivore coprolites fragments<br>• Granostriated b-fabric<br>• Very low amounts of fire residues, lithics, and shells<br>• Bioturbation | Reduced human activity in the cave along with increase in carnivore activity |
| VII | MP | Loamy light brown | • Calcitic-clay groundmass cemented with secondary calcite<br>• Silt to medium sand size sub-angular quartz at 10% abundance<br>• Bone fragments in various colors ranging from yellow to white, some with masked birefringence, some calcined<br>• Dark brown-reddish clay-rich aggregates<br>• Low amounts of phosphatic grains<br>• High abundance of fire residues, lithics, and shells (some transformed from aragonite to calcite)<br>• Granostriated b-fabric<br>• Bioturbation | Human activity, associated with pyrogenic activity |

temperatures (Table 5 and Fig. 6b). Samples collected at the contact between AH III and IV were designated as transition III-IV, though most of them seems to show microscopic features similar to AH III and might represent some mixing with the underlying AH IV (Table 4 and Fig. 5).

## AH IV

The sediments analyzed from AH IV exhibit a complex microstructure with calcitic-clay groundmass. The quartz found at 10% abundance is sub-angular and of silt to medium-sand size. Granostriated b-fabric is found around quartz grains as well as around chert and bone fragments. Most prominently, compared with the other layers, AH IV displays a high abundance of phosphatic grains along with larger coprolite fragments and chewed and digested bones (Table 4 and Figs. 5 and 9). While some fire residues were observed, overall they are found in low abundance (Table 4 and Fig. 9d–e). Limestone from the lower part of this layer shows signs of dissolution. Clay minerals analyzed using micro-FTIR indicated high O–H absorption bands at 3620 and 3695 $cm^{-1}$, which is associated with unaltered clay (Table 5 and Fig. 6c). However, FTIR analysis of bulk sediment samples from AH IV reveals a mixed assemblage of unaltered and heat-altered clay, bones, and shells (Table 2). Samples collected at the contact between AH IV and V were designated as transition IV–V, though most of them seems to show microscopic features similar to AH IV and might represent some mixing with the underlying AH V (Table 4 and Fig. 5).

## AH V

The microstructure of AH V sediments is complex and massive, with many channels, vesicles, vughs, and chambers. Quartz is sub-angular displaying silt to medium-sand size at 10% abundance. A very high proportion of micro-charcoals, wood ash pseudomorphs, burnt bones, reddish clay aggregates, lithics, shells, and bone fragments is found within a cemented matrix (Table 4 and Fig. 5). Limestone fragments within the sediments display dissolution. This in turn resulted in the precipitation of secondary calcite cementing the matrix, which itself is composed of a groundmass dominated by clay and in some cases shows evidence of manganese staining (Fig. 10a–b). In some areas, phosphatization occurred associated with the dissolution of calcite, probably as more acidic conditions formed locally (Fig. 10c–e). Bones range in color from yellow and white to orange; some show manganese staining, and some are associated with wood ash (Fig. 10f–g). Further indication of fire residues is found in the form of dark reddish-brown clay-rich aggregates (Fig. 10a–b). These show signs of heat-alteration based on micro-FTIR analysis indicating the absence of O–H absorption bands at 3620 and 3695 $cm^{-1}$ (Table 5 and Fig. 6d and e, respectively). FTIR analysis of this layer indicates high

**Table 4** Qualitative analysis of relative abundance of key micromorphological features in thin sections, sorted by layer and then elevation. (- = not observed in thin section; * = qualitative observation of the abundance in relation to the other thin sections from the site)

| Thin section | Square | Profile | Elevation | Layer | Cementation | Phosphatic grains | Fire residues | Bones | Lithics | Shells |
|---|---|---|---|---|---|---|---|---|---|---|
| 13-4A | G50 | North | 6.18 | II | - | ** | ** | *** | ** | * |
| 13-4B | G50 | North | 6.18 | II | - | ** | ** | *** | * | * |
| 13–3 | G50 | North | 6.25 | III | * | * | ** | *** | ** | - |
| 15-9A | H50 | South | 6.10 | III | * | * | ** | ** | * | * |
| 15-9B | H50 | South | 6.00 | III | * | * | ** | *** | ** | ** |
| 13–2 | G50 | North | 6.09 | III–IV | * | * | ** | *** | ** | * |
| 15-5A | H51 | North | 6.05 | III–IV | * | * | ** | ** | * | * |
| 15-9C | H50 | South | 5.87 | III–IV | * | ** | ** | *** | ** | ** |
| 14-4A | G51 | East | 6.21 | IV | ** | * | * | ** | * | - |
| 13-4B | G50 | North | 6.18 | IV | * | ** | * | *** | - | - |
| 15-1A | G51 | West | 6.11 | IV | ** | *** | * | ** | ** | * |
| 14-3A | H50 | North | 6.03 | IV | ** | *** | * | *** | * | - |
| 13-5A | G50 | North | 6.01 | IV | * | ** | * | ** | * | * |
| 13-5B | G50 | North | 6.01 | IV | * | ** | * | ** | * | * |
| 13–1 | G50 | North | 6.01 | IV | ** | *** | - | *** | * | - |
| 15-1B | G51 | West | 6.00 | IV | ** | *** | * | ** | ** | * |
| 15-5B | H51 | North | 5.97 | IV | ** | ** | * | * | - | - |
| 15-8A | G49 | East | 5.46 | IV | ** | **** | - | * | - | - |
| 13-5A | G50 | North | 6.01 | IV–V | ** | ** | * | ** | * | * |
| 13-5B | G50 | North | 6.01 | IV–V | ** | ** | * | ** | * | * |
| 14-4B | G51 | East | 5.98 | IV–V | ** | *** | * | *** | * | - |
| 17-1A | I49 | North | 5.73 | IV–V | **** | ***** | * | **** | - | - |
| 17-1B | I49 | North | 5.65 | IV–V | **** | ***** | * | **** | * | - |
| 17-1C | I49 | North | 5.57 | IV–V | **** | ***** | * | **** | ** | * |
| 14-3A | H50 | North | 6.00 | V | **** | *** | *** | *** | *** | ** |
| 13–1 | G50 | North | 6.01 | V | **** | ** | *** | *** | ** | ** |
| 15-1B | G51 | West | 6.00 | V | **** | * | * | ** | ** | * |
| 15-6A | H51 | North | 5.91 | V | *** | * | *** | *** | ** | ** |
| 15-1C | G51 | West | 5.90 | V | **** | * | ** | ** | ** | * |
| 14-3B | H50 | North | 5.85 | V | **** | * | **** | *** | *** | ** |
| 15–10 | H50 | South | 5.80 | V | *** | ** | *** | *** | ** | ** |
| 15-6B | H51 | North | 5.74 | V | *** | * | **** | *** | *** | ** |
| 15-2B | G51 | West | 5.71 | V | **** | * | **** | *** | *** | ** |
| 15-7A | H50 | North | 5.74 | V | **** | * | **** | **** | **** | *** |
| 15-7B | H50 | North | 5.60 | V | **** | ** | **** | **** | **** | *** |
| 15-3A | G51 | West | 5.74 | V | **** | * | *** | ** | ** | * |
| 15-3B | G51 | West | 5.64 | V | **** | * | *** | ** | ** | * |
| 15-4A | G50 | North | 5.62 | V–VI | *** | * | * | * | * | - |
| 15-4B | G50 | North | 5.50 | VI | *** | ** | * | * | - | - |
| 15-4C | G50 | North | 5.39 | VI | *** | ** | * | * | * | - |
| 15-8A | G49 | East | 5.46 | VI | *** | **** | - | *** | - | - |
| 15-8B | G49 | East | 5.30 | VI | ** | **** | - | ** | - | - |
| 15-8C | G49 | East | 5.21 | VI | **** | ***** | ** | ** | * | * |
| 17-2A | G49 | South | 5.38 | VI | *** | ***** | - | *** | - | - |
| 17-2B | G49 | South | 5.02 | VI | *** | ***** | - | *** | - | - |
| 17-3A | G49 | East | 5.15 | VII | **** | * | **** | *** | *** | ** |
| 17-3B | G49 | East | 4.97 | VII | **** | * | **** | *** | *** | ** |

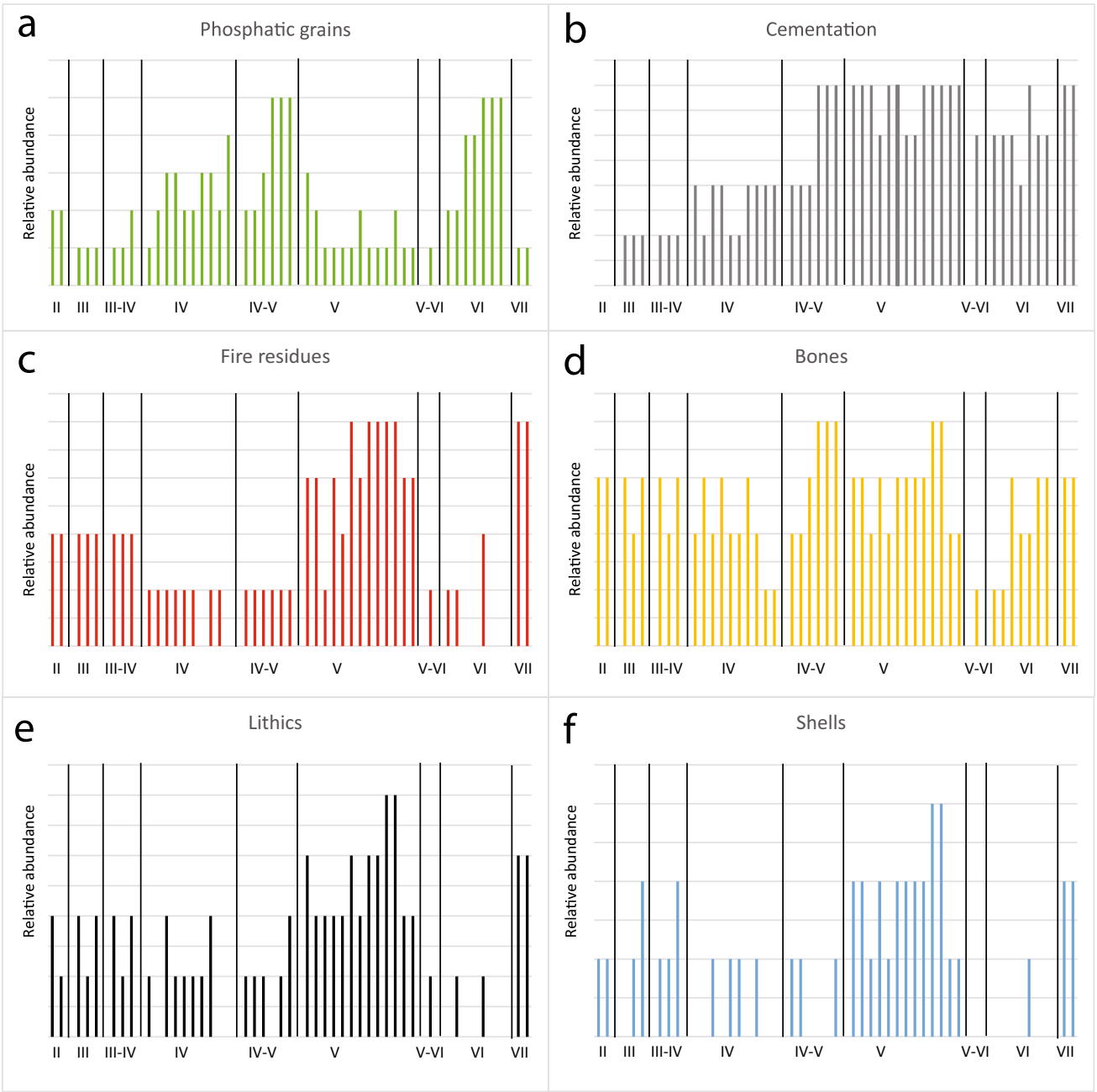


**Fig. 5** Qualitative assessment of microscopic features in thin sections (each bar represent part of a thin section ordered according to stratigraphic position). **a** Relative abundance of phosphatic grains. **b** Relative extent of calcitic cementation of the matrix. **c** Relative abundance of fire residues including rubified clay aggregates, micro-charcoal, wood ash pseudomorphs and burnt bones. **d** Relative abundance of microscopic bones (<2 mm). **e** Relative abundance of chert fragments. **f** Relative abundance of shells

numbers of calcined bones as well as shells being transformed from aragonite to calcite, typical for burnt shells (Table 2 and Fig. 4d–e).

## AH VI

Under the microscope, the layer displays calcitic-clay groundmass with complex microstructure dominated mainly by channels along with chambers, vughs, and vesicles. Silt to medium-sand sized sub-angular quartz is found at 10% abundance. Overall, the layer is quite similar to AH IV, showing high abundance of phosphatic grains and low abundance of fire residues, lithics, and shells (Table 4 and Figs. 5 and 11). The extent of calcitic cementation of the matrix appears higher than in AH IV but somewhat less than in AH V (Table 4 and Figs. 5, 7f). FTIR analysis identified a few calcined bones

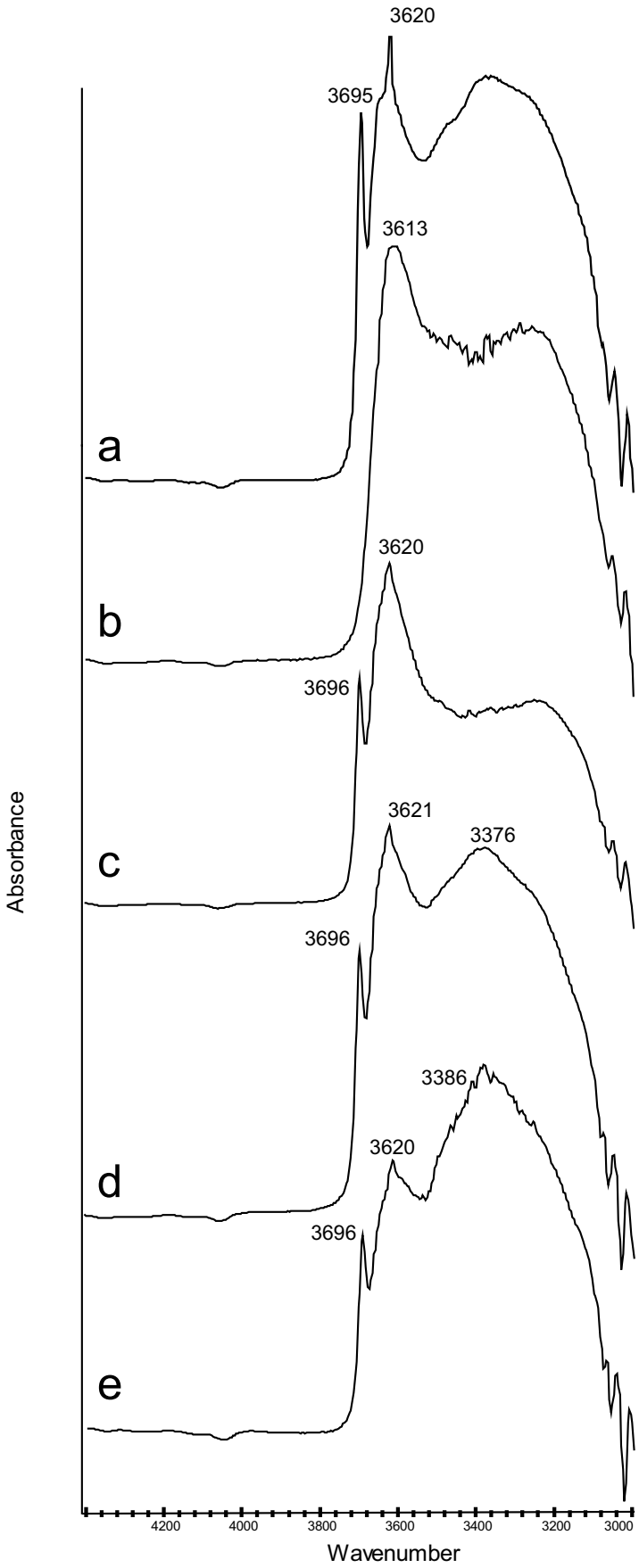


**Fig. 6** Spectra obtained through micro-FTIR analysis under transmission mode at 4 $cm^{-1}$ resolution. Note that because of the presence of glass and resin, absorption under 3000 $cm^{-1}$ was excluded. **a** Regional *terra rossa* collected above the cave. Note the presence of prominent absorption bands at 3695 and 3620 $cm^{-1}$ indicative of unaltered clay. **b** Dark colored clay-rich aggregate in Layer III. Note the absence of the absorption band at 3695 $cm^{-1}$, which may suggest the alteration of the clay minerals due to exposure to temperatures higher than 450 °C. **c** General matrix of layer IV. **d** General matrix of layer V. **e** Dark colored clay-rich aggregate in layer V. Note the reduced height of absorption bands at 3695 and 3620 $cm^{-1}$ in comparison to the general matrix in the same layer. Yet, the clay minerals do not show clear indications of alteration due to exposure to temperatures higher than 450 °C

**Table 5** Results of micro-FTIR analysis of clay components in thin sections sorted by layer. The table displays the presence/absence of absorption bands at 3620 and 3695 cm-1 used for interpreting pyrogenic alteration of clay

| Thin section | Square | Profile | Layer | Description | Height of H-O peaks | Interpretation |
|---|---|---|---|---|---|---|
| 14-1 | Control | | | General matrix | High | Unburnt |
| 13-4A | G50 | North | II | General matrix | Reduced | Slightly burnt or mixed |
| 13-4A | G50 | North | II | General matrix | Reduced | Slightly burnt or mixed |
| 13-3 | G50 | North | III | General matrix | High | Unburnt |
| 13-4 | G51 | North | III | Clay aggregate | No peaks | Burnt |
| 13-5 | G52 | North | III | Clay aggregate | High | Unburnt |
| 13-5A | G50 | North | IV-V | General matrix | High | Unburnt |
| 13-5A | G50 | North | IV-V | General matrix | High | Unburnt |
| 14-3B | H50 | North | V | General matrix | Medium | Unburnt |
| 14-3B | H50 | North | V | General matrix | Medium | Unburnt |
| 14-3B | H50 | North | V | Clay aggregate | Reduced | Slightly burnt or mixed |
| 15-2B | G51 | West | V | Clay aggregate | Reduced | Slightly burnt or mixed |
| 15-2B | G51 | West | V | Clay aggregate | Reduced | Slightly burnt or mixed |
| 15-3A | G51 | West | V | Clay aggregate | No peaks | Burnt |
| 17-2B | G49 | South | VI | Clay aggregate | Reduced | Slightly burnt or mixed |
| 17-2B | G49 | South | VI | Clay aggregate | Reduced | Slightly burnt or mixed |
| 17-3A | G49 | East | VII | Clay aggregate | High | Unburnt |
| 17-3A | G49 | East | VII | Clay aggregate | Reduced | Slightly burnt or mixed |

as well as shells and clay aggregates altered by exposure to elevated temperatures (Table 2). Dark clay aggregates analyzed by micro-FTIR indicate reduced levels of O–H absorbance bands, suggesting either mixed or slightly burnt clays (Table 5).

### AH VII

This layer's microstructure is complex with channels, chambers, vughs and vesicles (Fig. 7g). Bone fragments are found in various colors ranging from yellow to white, some with masked birefringence (possibly from charring) and some calcined (Table 2). Sediments are highly cemented by secondary calcite showing calcitic-clay groundmass with silt to medium-sand sized sub-angular quartz found at 10% abundance and a high abundance of fire residues (e.g., calcined bones, rubified clay aggregates, micro-charcoal, and ash) (Table S3, Figs. 5 and 12). The dark clay aggregates analyzed using micro-FTIR indicate high levels of O–H absorbance bands in one case, suggesting unburnt clays, while in another, the bands are reduced, suggesting mixed or slightly burnt clays (Table 5).

## Discussion

### Site formation processes

*Terra rossa* composes the major source of sediments in the renewed excavation area at the entrance of the cave. This locally formed soil was deposited in the cave through colluvial processes. The sub-angular silt to medium-sand sized quartz indicates an additional contribution of wind-blown material from the nearby coastal plain. This was also observed by Farrand (1984), who suggested that the mixture between the colluvial *terra rossa* and the aeolian quartz occurred in situ within sediments of the cave and terrace. Nonetheless, we also identified sub-angular silt to fine sand-sized quartz in the control samples from above the cave. Thus, it is possible that some of the quartz was first deposited outside the cave, mixed with the *terra rossa*, and then transported together into the cave by gravity as reported in many caves in the Southern Levant (Goldberg 1973; Frumkin et al. 2009, 2016; Friesem et al. 2019, 2021a; Berna et al. 2021). The relatively constant amount of silt across the sequence, despite the changing nature of the opening of the cave following a series of collapses, further supports it resulting from prime mixing of the soil on the plateau above prior to its colluvial deposition in the cave. This interpretation is also supported by indications of syn-depositional processes such as the complex microstructure of the sediments dominated by channels (Table 3 and Fig. 7), along with the presence of coatings on grains and aggregates as well as chert and bone fragments with granostriated b-fabric around them (Figs. 8 and 9b). This feature likely results from rotational deformation during emplacement of the deposits (Stoops 2003; Mücher et al. 2018).

Signs of minor to moderate disturbance in the deposits due to biological activity (e.g., roots, microfauna, nesting, and burrowing) and processes of diagenesis are evident

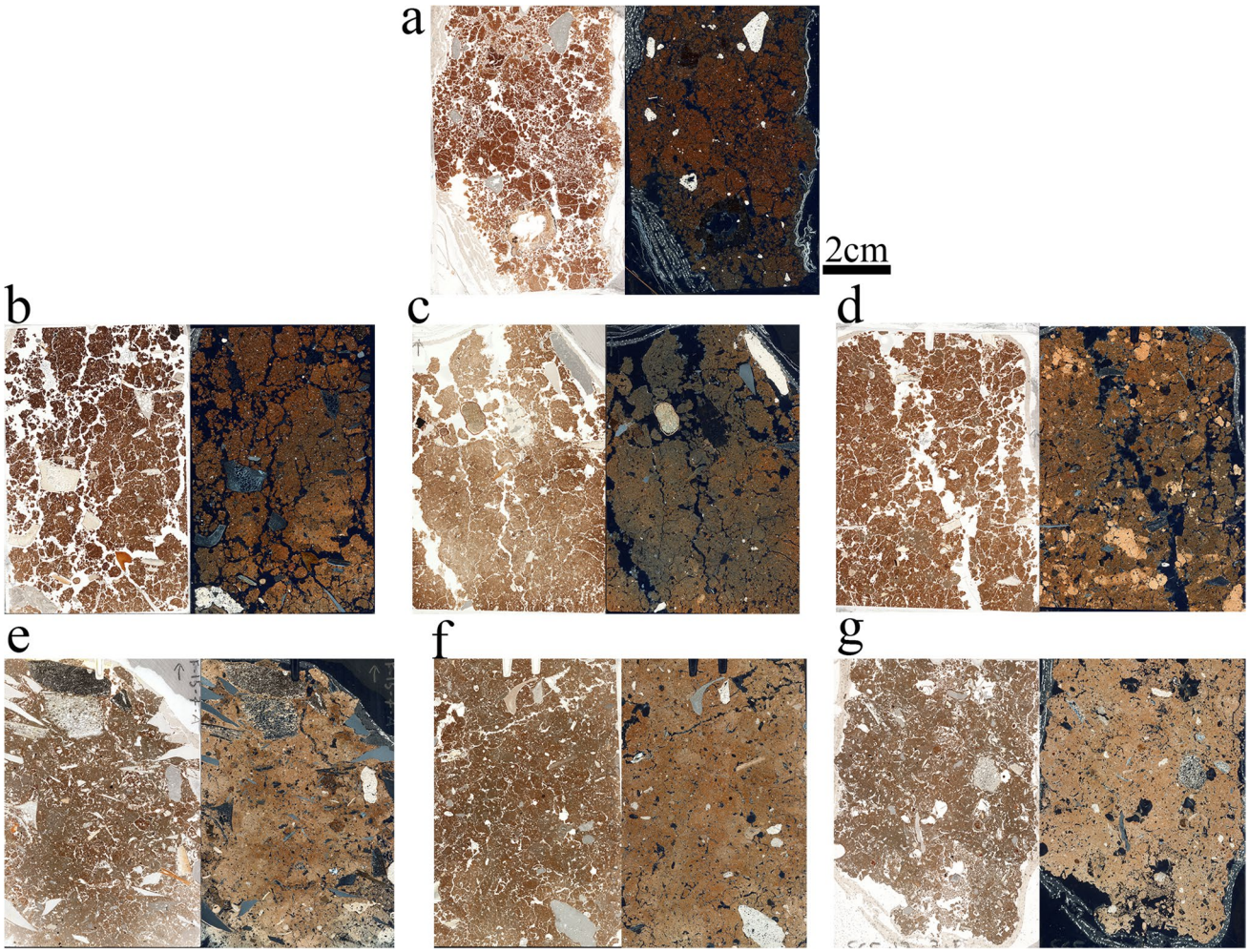


**Fig. 7** Scans of representative thin sections in PPL (left) and XPL (right) view. **a** Regional *terra rossa* sediment showing red-brown rounded peds with open microstructure. **b** Layer II displaying a clay-rich matrix with a complex microstructure dominated by large channels. Note that besides a few limestone fragments, the sediment is overall decalcified. **c** Layer III showing a clay-rich matrix, decalcified in most areas with complex microstructure and high abundance of chert and bone fragments (some burnt). **d** Layer IV presenting a calcitic-clay matrix with high abundance of coprolite fragments. **e** Layer V exhibiting dense matrix rich in calcite with very high abundance of chert fragments and fire residues. **f** Layer VI showing dense calcitic-clay matrix with reduced concentrations of lithics, fire residues and shells, and elevated concentration of phosphatic grains. **g** Layer VII presenting a cemented matrix with high abundance of fire residues, lithics, and shells

throughout the sedimentary sequence. The major post-depositional processes at Sefunim Cave include decalcification of the upper layers (AH II–III) followed by precipitation of secondary calcite which gradually cements the sediment matrix of the lower layers (AH V–VII) (see also Farrand 1984). While we do not observe major alterations of the (macro-)archaeological materials (bones, charcoal, lithics, shells, etc.), this might affect the radiometric dating samples that are accompanied by dosimetry control (Mercier and Valladas 2003; Weiner 2010). On the one hand, AH IV shows dissolution of limestone, but also a gradual increase of secondary calcite cementing the matrix, which increases with depth. Accordingly, many of the finds of AH V–VII are partially covered by crust of the same nature. Nonetheless, micromorphological observations indicate that AH V shows a very high degree of cementation, with AH VI being less cemented (Tables 3 and 4, Fig. 5). Thus, a further source of secondary calcite seems to have enhanced the cementation of the matrix in AH V. We attribute the second source to a high abundance of dissolved calcitic wood ash (Fig. 10f–g). Phosphatization associated in part with the dissolution of limestone (Fig. 10c–e) provides another indication of the presence of ash (e.g., Schiegl et al. 1996). Finally, parts of AH VII exhibit a similar degree of cementation as in AH V (Table 4 and Fig. 5). Altogether, the sequence of AH V-VII provides an excellent example of how two factors—(1) decalcification and reprecipitation of calcite and (2) deposition of calcitic ash—contributed to the cementation

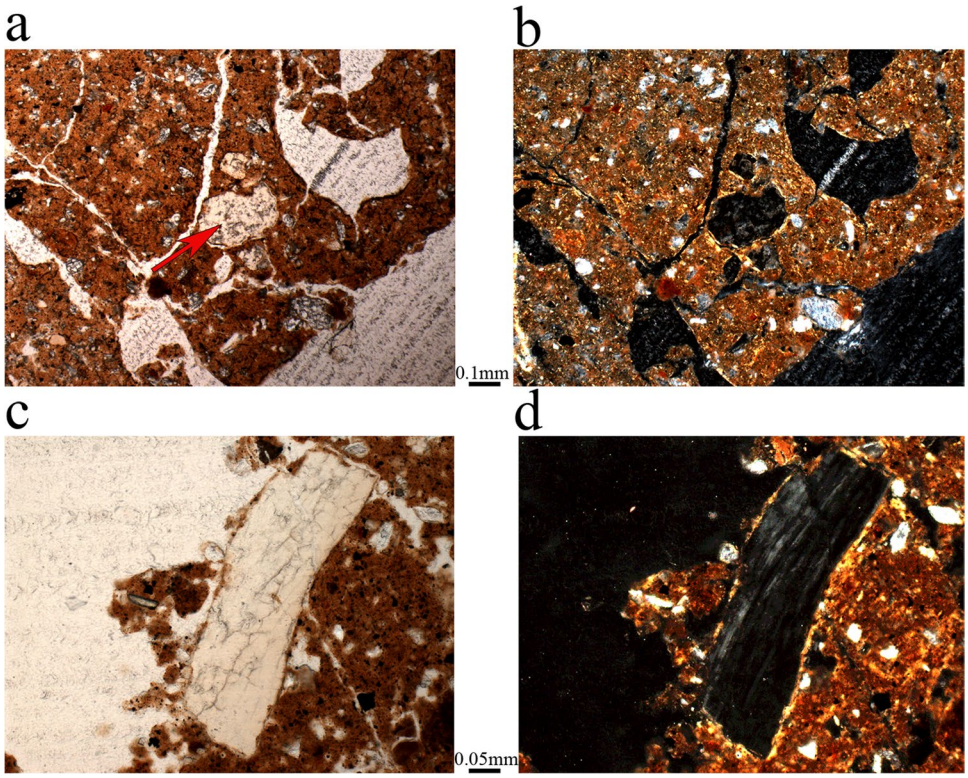


**Fig. 8** Microphotographs of layer III. **a** The general matrix of the sediment showing clay rich matrix mostly decalcified and with silt to medium-sand size sub-angular quartz at 5–10% abundance. Note the phosphatic grain (red arrow). Microphotograph taken in PPL. **b** Same microphotograph in XPL showing granostriated b-fabric around the phosphatic grain. **c** Close up of a bone fragment taken in PPL. **d** Same microphotograph in XPL showing granostriated b-fabric around the bone fragment

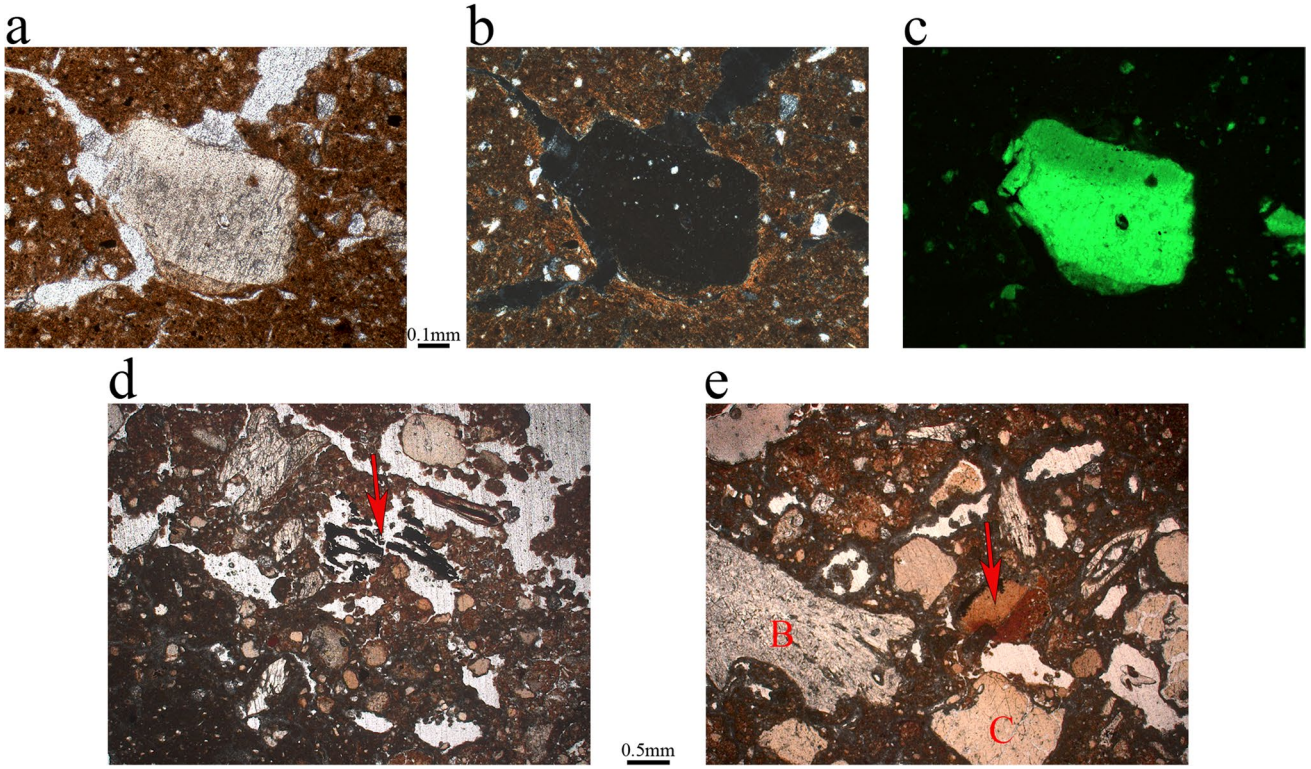


**Fig. 9** Microphotographs of layer IV. **a** A fragment of a carnivore coprolite showing massive structure composed of apatite with round voids. Microphotograph taken in PPL. **b** Same microphotograph in XPL showing granostriated b-fabric around the coprolite. **c** Same microphotograph under blue-light fluorescence. Note the spatial abundance of microscopic phosphatic grains. **d** Mixed assemblage showing calcite rich cemented area (bottom left corner) with multiple phosphatic grains and charred remains (red arrow). **e** Mixed assemblage showing chewed and digested bone (B), coprolite fragment (C) and burnt bone fragment (red arrow)

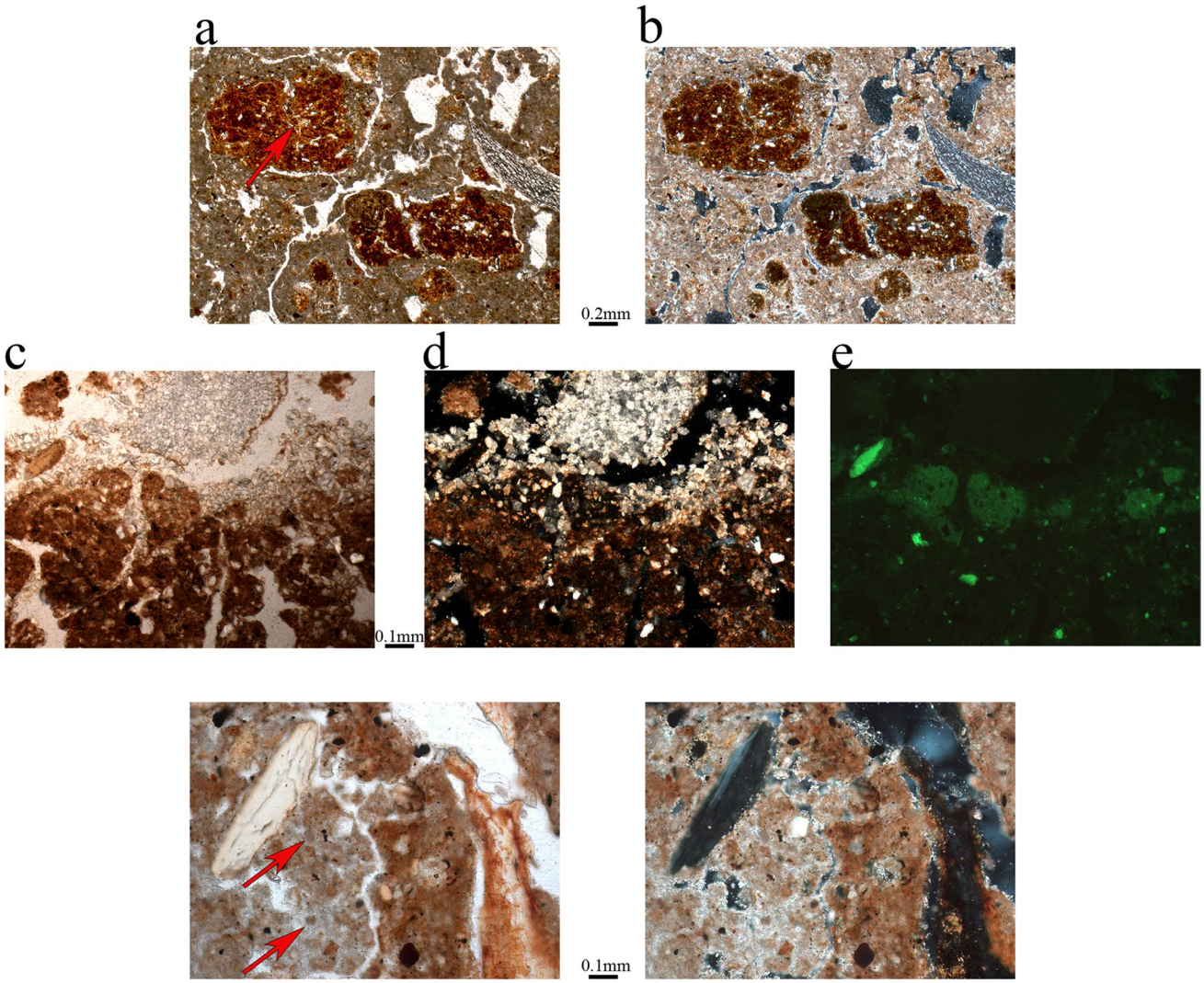


**Fig. 10** Microphotographs of layer V. **a** The general matrix of the sediment shows secondary calcite cementing the groundmass. The red arrow marks the dark colored (rubified) clay-rich aggregate, which under the microFTIR shows alteration due to exposure to elevated temperatures, taken in PPL. **b** Same microphotograph in XPL. **c** Limestone dissolution with phosphatization, taken in PPL. **d** Same microphotograph in XPL. **e** Same microphotograph under blue-light fluorescence. f A bone embedded in cemented calcite-rich matrix with calcitic wood ash pseudomorphs (red arrows), taken in PPL. g Same microphotograph taken in XPL

processes. It also demonstrates the benefit of tracing the history of each factor separately.

The dissolution of limestone is a widely reported phenomenon in Paleolithic caves associated with wet and acidic conditions (Goldberg and Sherwood 2006; Mallol and Goldberg 2017). Many MP and UP caves in the Southern Levant reported leaching of limestone associated with diagenesis following the decomposition of bat and bird guano (Goldberg and Nathan 1975; Goldberg and Bar-Yosef 1998; Karkanas et al. 2000; Shahack-Gross et al. 2004; Friesem et al. 2019). Yet, we did not identify the extensive presence of authigenic phosphate minerals. On the other hand, we did observe clearly defined phosphatic grains attributed to coprolite fragments or localized decomposition of organics, which we would expect if diagenesis followed guano decomposition (Karkanas et al. 2000; Karkanas 2017; Karkanas and Goldberg 2018; Friesem et al. 2021a, b). Therefore, we conclude that the dissolution of calcite and its reprecipitation is associated with wet and slightly acidic (pH 6–7) conditions.

The gradual collapse of the cave's roof near its entrance represents a major alteration of the study area. This process deposited limestone boulders onto exposed deposits at various times. For example, the massive "Three-Drill Rock" found in the upper part of AH III marks an episode of collapse during the Late Pleistocene. Further evidence comes from roof fragments including stalactites, which we found mainly in AH V and less frequently in AH IV.

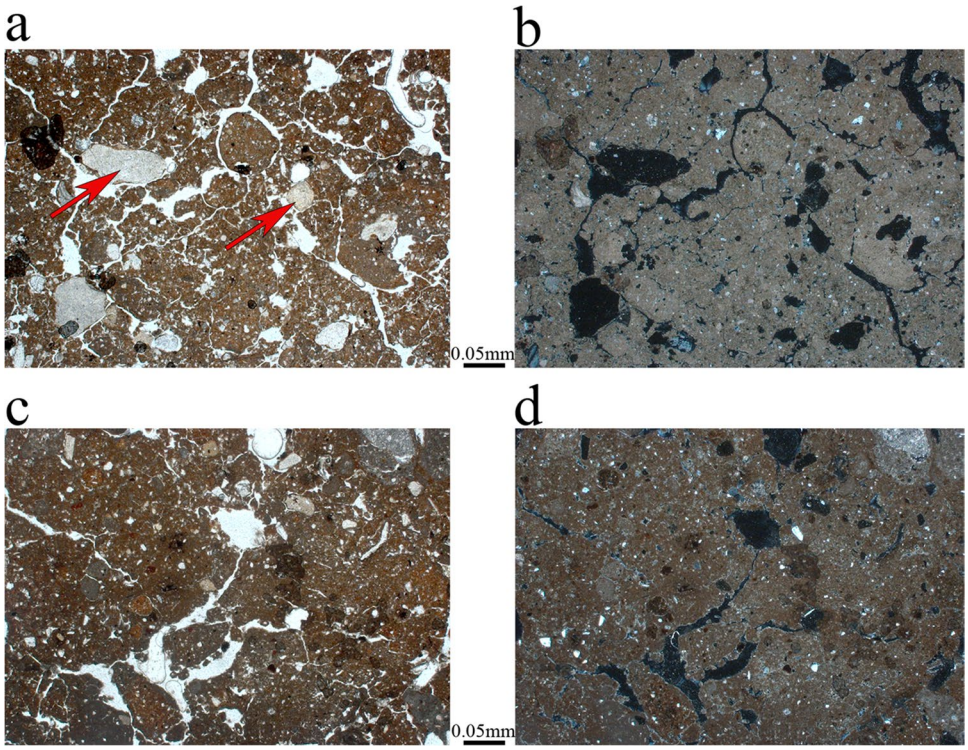


**Fig. 11** Microphotographs of layer VI. **a** General matrix showing calcitic-clay groundmass with high abundance of phosphatic grains (red arrows), taken in PPL. **b** Same microphotograph in XPL. Note the high content of calcite cementing the matrix. **c** General matrix showing phosphatic grains mixed with cemented areas (dark gray) and dark reddish clay aggregates (possibly altered), taken in PPL. **d** Same microphotograph in XPL. Note higher clay content in the groundmass

The presence of stalactite fragments suggests that this area was not at the entrance of the cave as it is today. A major episode of roof collapse occurred post-AH III, probably during the Holocene (see also Ronen 1984). This event changed the cave's configuration by opening up the cave to the elements and exposing the deposits that are now located at the entrance. In this way, the *terra rossa* deposited close to the cave's entrance (AH I-III) was exposed to greater amounts of rainwater after this rockfall, enhancing the process of decalcification (Mallol and Goldberg 2017).

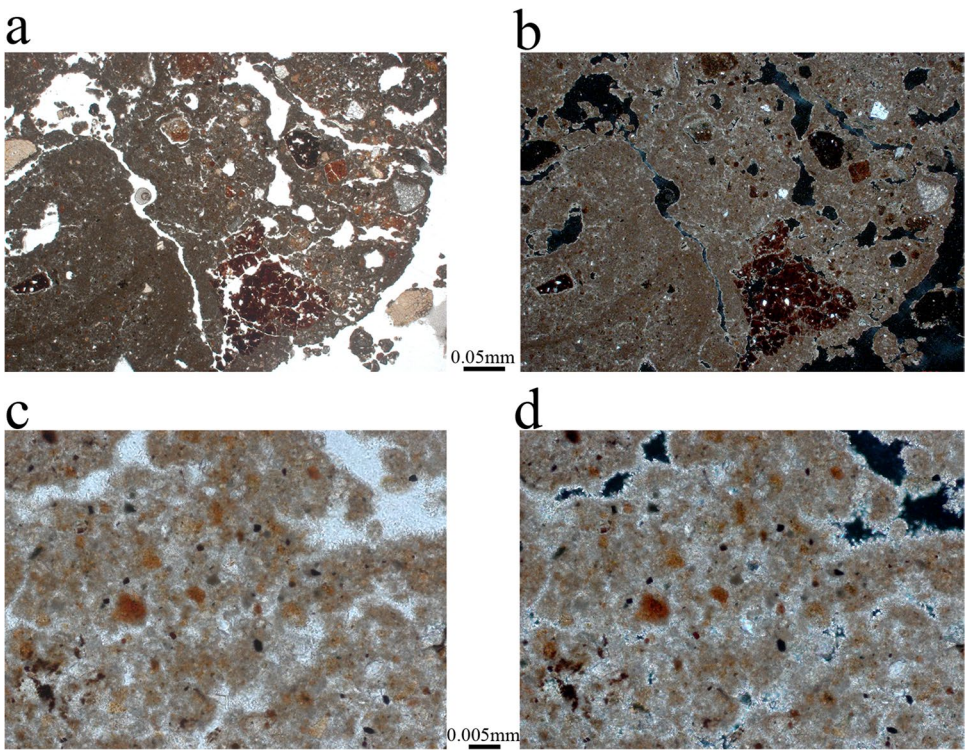


**Fig. 12** Microphotographs of layer VII. **a** Highly cemented matrix with rubified clay aggregates, micro-charcoal, and ash mixed with a few phosphatic grains, taken in PPL. **b** Same microphotograph taken in XPL. **c** Close up showing abundance of cemented wood ash, taken in PPL. **d** Same microphotograph taken in XPL

## Human and Animal activity at Sefunim Cave

The use of caves by humans and carnivores during the Late Pleistocene is reported at several sites in the Southern Levant (Speth and Tchernov 2007; Friesem et al. 2019; Orbach and Yeshurun 2021; Barzilai et al. 2021) and elsewhere in Eurasia and Africa (Stiner et al. 1996; Zilio et al. 2021). These studies demonstrate alternating occupations by human and carnivores as well as the difficulties of separating them within the palimpsests that often characterize cave deposits. Markers for both human and animal activity in the cave are found in almost all of the cave's deposits. However, their intensity seems to alternate stratigraphically, displaying reverse correlation between two relative sets of conditions. The first set indicates an abundance of carnivore activity including coprolite fragments, phosphatic grains, and bones showing signs of weathering and chewing (Horwitz and Goldberg 1989; see Friesem et al. 2019). Although, based on micromorphology alone, we cannot unequivocally identify small phosphatic grains as carnivore coprolite fragments, their abundance is found in direct relation to other, larger grains that do display clear characteristics of having derived from carnivore coprolites. These include, for example, larger phosphatic grains showing clear evidence of coprolite fragments, e.g., morphology of voids (see Fig. 9a), digested and chewed bones (Horwitz and Goldberg 1989). Our interpretation is also echoed through other studies and finds, including the recovery of hyena aDNA from the sediments at Sefunim, as well as complete coprolites and bones derived from hyenas (Slon et al. 2022). The second set confirms the abundance of human activity as seen by fire residues (e.g., micro-charcoal, calcined bones, rubified clay aggregates, calcitic wood ash pseudomorphs, and shells transformed from aragonite to calcite due to burning), chert fragments, and shells (although the latter could just indicate the natural presence of land snails) (Table 4 and Fig. 5). The alteration of clay within *terra rossa* aggregates and the calcined bones indicate their exposure to relatively high temperatures (> 500 °C). Even though in situ combustion features were not discovered during excavation, the direct relation between the presence of fire residues and increased abundance of lithics and shells further supports the interpretation of anthropogenic use of fire, as opposed to natural wild fire.

Based on the micro-archaeological record and relative abundance of markers of human and animal activity within it, we interpret the sedimentary sequence at Sefunim Cave as follows (see also Table 3):

- AH II: disturbed and mixed features, identified as pits (only pit IIa examined in this study)
- AH III: highest intensity of human occupation, associated with use of fire
- AH IV: relatively short episodes of alternating activities of carnivores and humans
- AH V: very high intensity of human occupation, associated with use of fire, possible longer episodes of occupation
- AH VI: carnivore activity and reduced human activity, possibly characterized by greater gaps between occupations
- AH VII: phase of increased human occupation whose intensity and distribution are not clear due to the limited extent of excavation in this layer

The geoarchaeological research, combined with the general findings about the site (Shimelmitz et al. 2018), indicates that AH III and V represent periods of more intense human occupation, while AH VII shows an increase in occupation compared to AH VI, though future excavations need to confirm this. The presence of coprolite fragments and phosphatic residues in varying degrees, including in the layers demonstrating intense human occupation, is a key to better understanding the human-carnivore relationship in the region. It is not a matter of alternating extremes, but rather a difference in the tempo and contribution of the agents characterizing each layer. In accordance with the results, we suggest that AH III and V represent more frequent and possibly longer or more intensive episodes of human occupation, alternating or interspersed with shorter phases of carnivores sporadically entering the cave. The likeliest candidate is hyena, based on coprolite fragments, taphonomic signs on bones, the analysis of the faunal assemblages, and aDNA evidence (Slon et al. 2022). AH IV and VI seem to reflect a mirror image, where carnivores appear to have occupied the cave more frequently, while humans arrived for shorter, more ephemeral episodes.

## Broader implications on human-carnivore relations

The evidence from Sefunim Cave shows clear evidence for both human and carnivore activity in an area that was close to the entrance of the cave. While not exceptional (e.g., in Manot Cave see Berna et al. 2021), this stands in contrast to other examples in Paleolithic caves of the Southern Levant, where carnivore presence is mostly associated with the rear part of the cave (e.g., Friesem et al. 2019; Orbach and Yeshurun 2021; Yeshurun et al. 2021). The micro-stratigraphic examination of the different layers at the entrance of Sefunim Cave reveals that neither a strict dichotomy nor a separation exists between markers of human activity and those of carnivores. Even in layers rich with anthropogenic finds, phosphatic grains are present, and vice versa (Table 4 and Fig. 5). Based on our results, we cannot rule out minor

post-depositional movement of materials between the different stratigraphic units. Nonetheless, the micromorphological evidence does not support major transport of materials post-depositionally. This observation does not contradict a degree of post-depositional movement of materials over short distances. Therefore, it is more likely that the assemblages instead represent close interaction between humans and carnivores at the site. In other words, the time between humans and animals coming into the cave was probably shorter than could be traced micro-stratigraphically.

The close association between residues associated with human activity and carnivores raises the question of whether some caves were just better suited to both humans and carnivores. Or it may be that the preference for these choices and conditions derives from a mutual selection and benefit. We do not assume that humans and carnivores dwelled in Sefunim Cave simultaneously, but suggest that they might have interacted indirectly. The presence of layers rich in bones and coprolite fragments but with a low abundance of fire residues, lithics, and shells invites two possible scenarios: (1) bones deposited by humans, with no evidence for the use of fire, rapidly followed by the presence of carnivores which deposited coprolites, or (2) bone deposition by carnivores as part of their hunting preferences (see Orbach and Yeshurun 2021). In the second case, we should ask ourselves whether carnivore activity at the site could have attracted humans who were searching for game or even scavenging with an emphasis on chasing away predators (e.g., O'Connell et al. 1988a, b). Based on our data, we cannot reconstruct the precise reality of human and animal interactions at this cave. Nevertheless, we argue that the evidence from Sefunim Cave begs us to consider the plausibility of competitive, maybe even reciprocal, relationships between the humans and carnivores who used caves during the Paleolithic.

Examining the evidence from several Neanderthal sites in France, Discamps et al. (2012) argued that hyenas and humans not only competed for prey (see also Dusseldorp 2013); they may also have competed over the sites themselves. This suggests that as far as hyenas could be attracted to sites to scavenge leftovers of human food, it is also possible that humans might be drawn to hyena dens for a similar purpose. Further research is required to better understand the implications of the cave as an important resource, and how it played a role in the environmental niche construction of both humans and animals during the Paleolithic. Several questions remain open. What is the effect of the cave configuration (e.g., entrance vs. rear, as a natural shelter) on its attraction to the different activities of humans and animals? Is the presence of hunting by-products (e.g., meat, skin, bones, marrow) brought to the site by humans—and possibly also by hyenas (Orbach and Yeshurun 2021)—attractive to both humans and carnivores? How does the cave configuration or the type of activities and their by-products exert pressure on humans and carnivores, especially when they have to partition the site in space and time? Were the relations between humans and carnivores mutual or unidirectional? We hope that our study will encourage future exploration of these aspects though a multi-scalar approach by integrating micro-chrono-spatial analysis with other lines of evidence.

## Conclusions

This micro-geoarchaeological study of the newly exposed sedimentary sequence at Sefunim Cave enabled us to refine the stratigraphy observed in the field. It also allowed us to demonstrate the usefulness of the micro-archaeological record to better understand patterns of site use and archaeological formation processes. We detected phases of human occupation based on the presence of fire residues (e.g., micro-charcoal, rubified clays, burnt bones and shells, and wood ash) directly associated with elevated concentrations of chert and shell fragments. We interpreted other layers that alternate or interfinger with the highly anthropogenic phases to display more pronounced carnivore activity, probably of hyena, based on the increased abundance of phosphatic grains, coprolite fragments, and chewed and digested bones. The reverse correlation between the abundance of human vs. carnivore activity, as well as the frequent interspersing of the two, illustrates the close relationship between humans and animals, which played out in the cave. Here, we demonstrate the usefulness of micro-geoarchaeology to provide new observations about patterns of deposition and the relationship between human and animal-related assemblages. It also allows us to use the record generated as a proxy for evaluating the temporal and spatial dimensions of such interactions. With the majority of studies examining human-carnivore interactions focusing on prey choice and possible competition over resources, future studies should further examine the interaction of humans and animals at Paleolithic sites by using a micro-stratigraphical approach.

**Acknowledgements** The excavations at Sefunim Cave were carried out under permits issued by the Israel Antiquity Authority (licenses G9/2013; G32/2014; G64/2015; G66/2017) and the National Parks and Nature Reserve Authority (licenses 3059/13; 4117/14; 5121/15; A052/17). We are deeply grateful to the late Avraham Ronen for his support of our project at Sefunim and to Paul Goldberg for sharing notes, data, and slides from his previous work at the site. We thank Panagiotis Kritikakis for sample preparation and Jamie Clark, Meir Orbach, and Naomi Porat for valuable discussions and comments on earlier drafts of this paper. Last, we thank the many students and volunteers who helped during the field excavations at the site.

**Funding** Open Access funding enabled and organized by Projekt DEAL. The work at the site and the analyses were funded by the Leakey Foundation and the Irene Levi Sala CARE Archaeological Foundation (R.S. and A.W.K.), with support from ROCEEH, Heidelberg Academy of Sciences & Humanities (A.W.K. and M.L.S.), and

the Zinman Institute of Archaeology, University of Haifa (R.S.). The geoarchaeological work at the site was supported by the University of Tübingen, Teach@Tübingen and Tübingen Reloaded programs (D.E.F. and C.E.M.).

## Declarations

**Conflict of interest** The authors declare no competing interests.



## References

Alex B, Barzilai O, Hershkovitz I et al (2017) Radiocarbon chronology of Manot Cave, Israel and Upper Paleolithic dispersals. Sci Adv 3:e1701450. https://doi.org/10.1126/SCIADV.1701450/SUPPL_FILE/1701450_SM.PDF

Barzilai O, Abulafia T, Shemer M et al (2021) Rediscovering Geula Cave: a Middle Paleolithic cave site in northern Mt. Carmel. Israel Quat Int 624:181–197. https://doi.org/10.1016/J.QUAINT.2021.03.007

Belfer-Cohen A, Goring-Morris N (2012) The earlier Upper Palaeolithic: a view from the Southern Levant. In: Otte M, Shidrang S, Flas D (eds) The Aurignacian of Yafteh Cave and its Context (2005–2008 Excavations). ERAUL 132, Liège, pp 127–136

Berna F, Behar A, Shahack-Gross R et al (2007) Sediments exposed to high temperatures: reconstructing pyrotechnological processes in Late Bronze and Iron Age Strata at Tel Dor (Israel). J Archaeol Sci 34:358–373. https://doi.org/10.1016/j.jas.2006.05.011

Berna F, Boaretto E, Wiebe MC et al (2021) Site formation processes at Manot Cave, Israel: interplay between strata accumulation in the occupation area and the talus. J Hum Evol 160:102883. https://doi.org/10.1016/J.JHEVOL.2020.102883

Discamps E, Delagnes A, Lenoir M, Tournepiche J-F (2012) Human and Hyena Co-occurrences in Pleistocene sites: insights from Spatial, Faunal and Lithic Analyses at Camiac and La Chauverie (SW France). J Taphon 10:291–316

Dusseldorp GL (2013) Neanderthals and Cave Hyenas: co-existence, competition or conflict? In: Clark JL, Speth JD (eds) Vertebrate Paleobiology and Paleoanthropology. Springer, Dordrecht, pp 191–208

Farrand WR (1984) Geology and sedimentology of the Cave of Sefunim. In: Ronen A (ed) Sefunim Prehistoric sites, Mount Carmel, Israel, 230th edn. BAR International Series, Oxford, pp 381–399

Forget MCL, Regev L, Friesem DE, Shahack-Gross R (2015) Physical and mineralogical properties of experimentally heated chaff-tempered mud bricks: implications for reconstruction of environmental factors influencing the appearance of mud bricks in archaeological conflagration events. J Archaeol Sci Reports 2:80–93. https://doi.org/10.1016/j.jasrep.2015.01.008

Friesem DE, Anton M, Waiman-Barak P et al (2020) Variability and complexity in calcite-based plaster production: a case study from a Pre-Pottery Neolithic B infant burial at Tel Ro'im West and its implications to mortuary practices in the Southern Levant. J Archaeol Sci 113:105048. https://doi.org/10.1016/j.jas.2019.105048

Friesem DE, Malinsky-Buller A, Ekshtain R et al (2019) New data from Shovakh cave and its implications for reconstructing Middle Paleolithic settlement patterns in the Amud Drainage, Israel. J Paleolit Archaeol 2:298–337. https://doi.org/10.1007/s41982-019-00028-2

Friesem DE, Shahack-Gross R, Weinstein-Evron M et al (2021a) High-resolution study of Middle Palaeolithic deposits and formation processes at Tabun Cave, Israel: Guano-rich cave deposits and detailed stratigraphic appreciation of Layer C. Quat Sci Rev 274:107203

Friesem DE, Teutsch N, Weinstein-Evron M et al (2021b) Identification of fresh and burnt bat guano and pigeon droppings in Eastern Mediterranean karstic cave sites based on micromorphological and chemical characteristics. Quat Sci Rev 274:107238. https://doi.org/10.1016/J.QUASCIREV.2021.107238

Frumkin A, Karkanas P, Bar-Matthews M et al (2009) Gravitational deformations and fillings of aging caves: the example of Qesem karst system, Israel. Geomorphology 106:154–164

Frumkin A, Langford B, Marder O, Ullman M (2016) Paleolithic caves and hillslope processes in south-western Samaria, Israel: environmental and archaeological implications. Quat Int 398:246–258. https://doi.org/10.1016/J.QUAINT.2015.05.064

Goldberg P (1973) Sedimentology, stratigraphy and palaeoclimatology of et-Tabun Cave. Carmel, Israel. University of Michigan, Ann Arbor, Mt

Goldberg P, Bar-Yosef O (1998) Site formation processes in Kebara and Hayonim caves and their significance in Levantine prehistoric caves. In: Akazawa T, Aoki K (eds) Neandertals and modern humans in Western Asia. Plenum, New York, pp 107–125

Goldberg P, Nathan Y (1975) The phosphate mineralogy of et-Tabun cave, Mount Carmel, Israel. Mineraological Mag 40:253–258

Goldberg P, Sherwood SC (2006) Deciphering human prehistory through the geoarcheological study of cave sediments. Evol Anthropol Issues, News, Rev 15:20–36

Goring-Morris N, Belfer-Cohen A (2006) A hard look at the "Levantine Aurignacian": how real is the taxon? In: Bar-Yosef O, Zilhão J (eds) Towards a Definition of the Aurignacian. Instituto Português de Arqueologia, Lisbon, pp 297–314

Horwitz LK, Goldberg P (1989) A study of Pleistocene and Holocene hyaena coprolites. J Archaeol Sci 16:71–94. https://doi.org/10.1016/0305-4403(89)90057-5

Karkanas P (2017) Guano. In: Nicosia C, Stoops G (eds) Archaeological soil and sediment micromorphology. Wiley, Chichester, UK, pp 83–89

Karkanas P, Bar-Yosef O, Goldberg P, Weiner S (2000) Diagenesis in prehistoric caves: the use of minerals that form in situ to assess the completeness of the archaeological record. J Archaeol Sci 27:915–929. https://doi.org/10.1006/jasc.1999.0506

Karkanas P, Goldberg P (2018) Phosphatic features. In: Stoops G, Marcelino V, Mees F (eds) Interpretation of micromorphological features of soils and regoliths, 2nd edn. Elsevier, Amsterdam, pp 323–346

Loftus E, Rogers K, Lee-Thorp J (2015) A simple method to establish calcite:aragonite ratios in archaeological mollusc shells. J Quat Sci 30:731–735. https://doi.org/10.1002/JQS.2819

Madejová J (2003) FTIR techniques in clay mineral studies. Vib Spectrosc 31:1–10. https://doi.org/10.1016/S0924-2031(02)00065-6

Mallol C, Goldberg P (2017) Cave and rock shelter sediments. In: Nicosia C, Stoops G (eds) Archaeological soil and sediment micromorphology. Wiley Blackwell, Chichester, pp 359–382

Mercier N, Valladas H (2003) Reassessment of TL age estimates of burnt flints from the Paleolithic site of Tabun Cave, Israel. J Hum Evol 45:401–409. https://doi.org/10.1016/j.jhevol.2003.09.004

Mücher H, van Steijn H, Kwaad F (2018) Colluvial and mass wasting deposits. In: Stoops G, Marcelino V, Mees F (eds) Interpretation of micromorphological features of soils and regoliths. Elsevier, Amsterdam, pp 21–36

O'Connell JF, Hawkes K, Jones NB (1988a) Hadza hunting, butchering, and bone transport and their archaeological implications. J Anthropol Res 44:113–161. https://doi.org/10.1086/JAR.44.2.3630053

O'Connell JF, Hawkes K, Jones NB (1988b) Hadza scavenging: implications for Plio/Pleistocene hominid subsistence. Curr Anthropol 29:356–363. https://doi.org/10.1086/203648

Orbach M, Yeshurun R (2021) The hunters or the hunters: human and hyena prey choice divergence in the Late Pleistocene Levant. J Hum Evol 160:102572. https://doi.org/10.1016/J.JHEVOL.2019.01.005

Ronen A (1984) Sefunim prehistoric sites, Mount Carmel. Israel BAR International Series, Oxford

Schiegl S, Goldberg P, Bar-Yosef O, Weiner S (1996) Ash deposits in Hayonim and Kebara Caves, Israel: macroscopic, microscopic and mineralogical observations, and their archaeological implications. J Archaeol Sci 23:763–781. https://doi.org/10.1006/JASC.1996.0071

Shahack-Gross R, Berna F, Karkanas P, Weiner S (2004) Bat guano and preservation of archaeological remains in cave sites. J Archaeol Sci 31:1259–1272

Shimelmitz R, Friesem DE, Clark JL et al (2018) The Upper Paleolithic and Epipaleolithic of Sefunim Cave, Israel. Quat Int 464:106–125. https://doi.org/10.1016/j.quaint.2017.05.039

Singer A (2007) The soils of Israel. Springer-Verlag, Berlin

Slon V, Clark JL, Friesem DE et al (2022) Extended longevity of DNA preservation in Levantine Paleolithic sediments, Sefunim Cave. Israel Sci Rep 12:14528. https://doi.org/10.1038/s41598-022-17399-2

Speth JD, Tchernov E (2007) The Middle Paleolithic occupations at Kebara Cave: a faunal perspective. In: Bar-Yosef O, Meignen L (eds) Kebara Cave, Mt. Carmel, Israel. The Middle and Upper Palaeolithic Archaeology. Part 1. American School of Prehistoric Research Bulletin 49. Peabody Museum of Archaeology and Ethnology, Cambridge, pp 165–260

Stekelis M (1961) Iraq el-Baroud, nouvelle grotte préhistorique au mont Carmel. Bull Res Counc Isr 10G:302–320

Stiner MC, Arsebük G, Howell FC (1996) Cave bears and paleolithic artifacts in Yarimburgaz Cave, Turkey: dissecting a palimpsest. Geoarchaeology 11:279–327

Stoops G (2003) Guidelines for analysis and description of soil and regolith thin sections. Soil Science Society of America Inc., Madison, WI

Surovell TA, Stiner MC (2001) Standardizing infra-red measures of bone mineral crystallinity: an experimental Approach. J Archaeol Sci 28:633–642. https://doi.org/10.1006/JASC.2000.0633

Thompson TJU, Gauthier M, Islam M (2009) The application of a new method of Fourier transform infrared spectroscopy to the analysis of burned bone. J Archaeol Sci 36:910–914. https://doi.org/10.1016/j.jas.2008.11.013

Thompson TJU, Islam M, Bonniere M (2013) A new statistical approach for determining the crystallinity of heat-altered bone mineral from FTIR spectra. J Archaeol Sci 40:416–422. https://doi.org/10.1016/J.JAS.2012.07.008

Toffolo MB, Boaretto E (2014) Nucleation of aragonite upon carbonation of calcium oxide and calcium hydroxide at ambient temperatures and pressures: a new indicator of fire-related human activities. J Archaeol Sci 49:237–248. https://doi.org/10.1016/J.JAS.2014.05.020

Villagran XS, Strauss A, Miller C et al (2017) Buried in ashes: site formation processes at Lapa do Santo rockshelter, east-central Brazil. J Archaeol Sci 77:10–34. https://doi.org/10.1016/j.jas.2016.07.008

Weiner S (2010) Microarchaeology: beyond the visible archaeological record. Cambridge University Press, Cambridge

Yeshurun R, Schneller-Pels N, Barzilai O, Marder O (2021) Early Upper Paleolithic subsistence in the Levant: zooarchaeology of the Ahmarian-Aurignacian sequence at Manot Cave. Israel J Hum Evol 160:102619. https://doi.org/10.1016/j.jhevol.2019.05.007

Zilio L, Hammond H, Karampaglidis T et al (2021) (2021) Examining Neanderthal and carnivore occupations of Teixoneres Cave (Moià, Barcelona, Spain) using archaeostratigraphic and intra-site spatial analysis. Sci Reports 111(11):1–20. https://doi.org/10.1038/S41598-021-83741-9